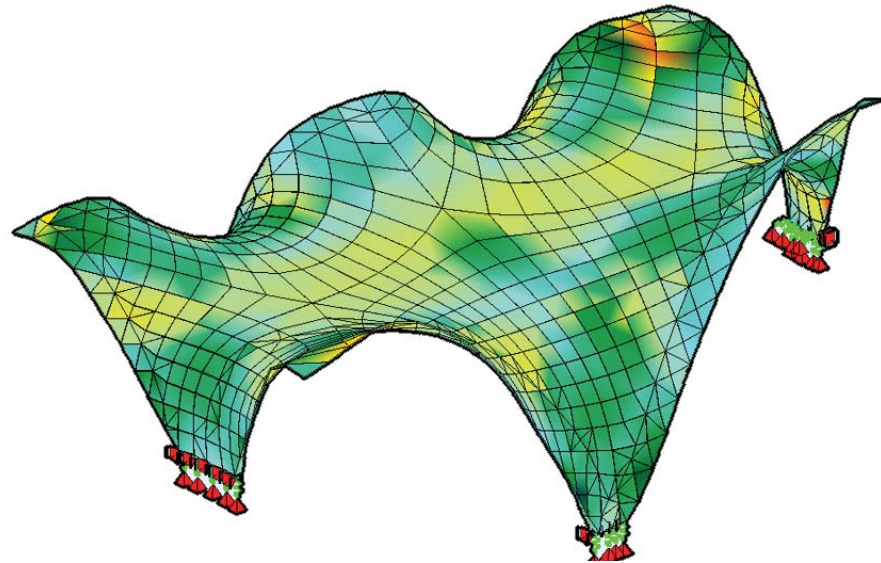




**LUND**  
UNIVERSITY



# ANALYSIS OF FERROCEMENT AND TEXTILE REINFORCED CONCRETE FOR SHELL STRUCTURES

MILE BEZBRADICA

Structural  
Mechanics

*Master's Dissertation*



DEPARTMENT OF CONSTRUCTION SCIENCES  
DIVISION OF STRUCTURAL MECHANICS

ISRN LUTVDG/TVSM--15/5207--SE (1-65) | ISSN 0281-6679

MASTER'S DISSERTATION

# ANALYSIS OF FERROCEMENT AND TEXTILE REINFORCED CONCRETE FOR SHELL STRUCTURES

MILE BEZBRADICA

Supervisor: Professor **KENT PERSSON**, Div. of Structural Mechanics, LTH.

Examiner: Professor **PER JOHAN GUSTAFSSON**, Div. of Structural Mechanics, LTH.

Cover image by kind permission of Block Research Group.

Copyright © 2015 Division of Structural Mechanics,  
Faculty of Engineering LTH, Lund University, Sweden.

Printed by Media-Tryck LU, Lund, Sweden, June 2015 (PI).

**For information, address:**

Division of Structural Mechanics,  
Faculty of Engineering LTH, Lund University, Box 118, SE-221 00 Lund, Sweden.

Homepage: [www.byggmek.lth.se](http://www.byggmek.lth.se)



## **Abstract**

The purpose of this master's thesis is to investigate the stiffness properties of three reinforcement materials for concrete shell structures: ferrocement, glass-fibre textile and carbon-fibre textile. Three types of strategies were used to analyse the properties of the materials, an analytical model, experimental beam prototypes and a numerical analysis. Immediate comparison of the mechanical experiments with the numerical models revealed stiffness deviations of 38% for the ferrocement, 272% for the glass and 211% for the carbon textile reinforced beam, respectively. Ferrocement is the stiffest material according to the mechanical tests. However, the results from the analytical and numerical models show that the carbon reinforced beam has the highest stiffness. Because of the disparity between results from the numerical and the mechanical model, the overall comparison is inconclusive. Possible causes are the influence of microcracks on the bond between the reinforcement and concrete as well as deviations of the concrete thickness of the physical samples. Future research should focus on assumptions in the material properties, numerical model and hand labour to be able to more properly investigate the actual stiffness of the three composite materials.

**Keywords:** SHELL STRUCTURES, FERROCEMENT, TEXTILE REINFORCED CONCRETE, FEM.



## Sammanfattning

Detta examensarbete undersöker styvhetsegenskaperna för tre armeringsmaterial: ferrocement, glasfiber- och kolfibertextilarmering, tillämpade för skalkonstruktioner. En av de strategier som användes för undersökningen var ett mekaniskt försök med kompositarmerade betongbalkar. Det mekaniska försöket skulle sedan verifieras med numeriska och analytiska modeller. Jämförelser mellan de mekaniska och numeriska resultaten gav avvikelser på 38 % för ferrocement, 272 % för glasfiberarmeringen respektive 211 % för kolfiberarmeringen. Enligt det mekaniska testet är ferrocement det styvaste materialet. Trots det visar resultaten från de analytiska och numeriska modellerna att kolfiberkompositen har den högsta styvheten. Slutsatsen utifrån detta är att antagandena från de numeriska och mekaniska studierna kan ha påverkats av vidhäftningsproblem mellan armering och betong. Dessutom kan resultaten också ha påverkats av de olika tvärsnittstjocklekarna på betongen från det mekaniska testet. Fokus på materialegenskaper, numerisk modellering och praktisk armeringsteknik krävs i framtida undersökningar för att styvheten för de tre kompositmaterialen ska kunna bestämmas.

**Nyckelord:** SKALKONSTRUKTIONER, FERROCEMENT, TEXTILARMERAD BETONG, FEM.



During five years of studying, this master's dissertation concludes my time at the civil engineering master program at Lund University. Many people have contributed in one way or another. I am very grateful of all of you; but there are some who deserve special thanks.

First of all, I would like to thank my supervisors, Diederik Veenendaal MSc and Prof. Dr Philippe Block. I am particularly pleased for introducing me to your projects and be a part of the Block Research Group at ETH Zurich (Swiss Federal Institute of Technology Zurich). I would like to thank Diederik especially for his endless assistance and support throughout this master's dissertation. I am looking forward to further collaborations in the future.

I would to thank my supervisor Prof. Kent Persson for your guidance and constructive criticism. Thank you for always having your door open and taking time to discuss the work. Furthermore, I would also thank Prof. Per Johan Gustafsson and my co-supervisor Vedad Alić MSc at the Division of Structural Mechanics for always being around to help me and discuss problems and new ideas.

I would like to thank a few people who have had an important part in making this dissertation possible. First of all, I would like to thank Mr Viktor Nilsson from Sto Scandinavia AB for helping me ordering the materials for the experiment. I would also thank Kristian Tammo PhD and Natalie Williams Portal Lic Eng from the Swedish Cement and Concrete Research Institute (CBI) for giving me the clues that caused exciting ideas and discussions.

I would also like to thank Prof. Lars Wadsö, Dr Katja Fridh, Mr Bengt Nilsson and Mr Per-Olof Rosenkvist at the Division of Building Materials for their help during the mechanical experiment. Special thanks go to Bengt and Per-Olof for helping me setting up this experimental program. In addition, I would like to thank several people at the Division of Structural Engineering for their feedback and comments. I am very thankful for the many discussions we had.

Finally, I would like to thank my family who always have supported me throughout the years. Hvala.

LUND, JUNE 2015



## Abbreviations and Symbols

$A$	Cross-sectional area	$m^2$
$A_{ef}$	Effective area	$m^2$
$E$	Young's modulus	$Pa$
$f_c$	Compression strength	$Pa$
$f_{cm}$	Mean compression strength	$Pa$
$f_t$	Tension strength	$Pa$
$f_{tu}$	Ultimate strength	$Pa$
$f_{ty}$	Yield tensile strength	$Pa$
$F$	Half of the axial point load $P$	$N$
$h_w$	Degree of hydration	%
$I$	Moment of inertia	$m^4$
$k$	Linear spring constant	$N/m$
$p_t$	Cement porosity	%
$P$	Axial point load	$N$
$P_c$	Axial crack load	$N$
$P_u$	Axial ultimate load	$N$
$q$	Lateral distributed load	$N/m$
$S$	Stiffness of parallel and serial spring models	$Pa$
$u$	Displacement	$m$
$w$	Airy stress function	—
$w/c$	Water-cement ratio	—
$\delta$	Deflection	$m$
$\epsilon$	Strain	—
$\nu$	Poisson's ratio	—
$\rho$	Density	$kg/m^3$
$\sigma$	Stress	$Pa$
$\tau$	Shear stress	$Pa$

$FE$     Finite element  
 $FEM$     Finite element method



# Contents

<b>1</b>	<b>Introduction</b>	<b>1</b>
1.1	Background . . . . .	1
1.2	Objective and Method . . . . .	1
1.3	Limitations . . . . .	2
1.4	Report Outline . . . . .	2
<b>2</b>	<b>Shell Structures</b>	<b>3</b>
2.1	Historical Review . . . . .	3
2.2	Current Projects . . . . .	4
2.3	Structure of a Shell . . . . .	4
2.3.1	Plate Theory . . . . .	5
2.3.2	Membrane Theory . . . . .	7
<b>3</b>	<b>Concrete Composites</b>	<b>9</b>
3.1	Concrete . . . . .	9
3.1.1	Definition . . . . .	9
3.1.2	Composition . . . . .	9
3.1.3	Physical Properties . . . . .	11
3.1.4	Mechanical Properties . . . . .	12
3.2	Ferrocement . . . . .	13
3.2.1	Definition . . . . .	13
3.2.2	Composition . . . . .	13
3.2.3	Physical Properties . . . . .	14
3.2.4	Mechanical Properties . . . . .	15
3.2.5	Applications . . . . .	15
3.3	Textile Reinforced Concrete . . . . .	16
3.3.1	Definition . . . . .	16
3.3.2	Composition . . . . .	16
3.3.3	Physical Properties of TRC . . . . .	18
3.3.4	Mechanical Properties of TRC . . . . .	18
3.3.5	Applications of TRC . . . . .	18
3.4	Comparison between Ferrocement and TRC . . . . .	19

<b>4</b>	<b>Mechanical Testing</b>	<b>21</b>
4.1	Experimental Program . . . . .	21
4.1.1	Preparation of Test . . . . .	22
4.1.2	Composition of the Specimens . . . . .	26
4.1.3	Method of Testing . . . . .	26
4.2	Results . . . . .	31
4.3	Discussion . . . . .	33
<b>5</b>	<b>Finite Element Model</b>	<b>37</b>
5.1	Finite Element Method . . . . .	37
5.1.1	Linear Elastic Analysis . . . . .	38
5.2	Abaqus . . . . .	38
5.3	Equivalent Models: RVE . . . . .	39
5.3.1	Geometry . . . . .	39
5.3.2	Material and Mesh . . . . .	39
5.3.3	D-matrix . . . . .	40
<b>6</b>	<b>Numerical Study of Mechanical Testing</b>	<b>45</b>
6.1	Finite Element Model . . . . .	45
6.1.1	Loads and Boundary Conditions . . . . .	45
6.1.2	Step and Mesh . . . . .	45
6.2	Results . . . . .	46
6.3	Discussion and Comparison with Mechanical Testing . . . . .	47
<b>7</b>	<b>Analytical Study of Numerical Model</b>	<b>49</b>
7.1	Stiffness of the Beam . . . . .	49
7.2	Mechanical Spring Models . . . . .	50
7.2.1	Serial Connected Model . . . . .	51
7.2.2	Parallel Connected Model . . . . .	52
7.3	Results . . . . .	53
7.4	Discussion and Comparison with Numerical Model . . . . .	54
<b>8</b>	<b>Comparison of Ferrocement and TRC</b>	<b>55</b>
8.1	Results . . . . .	55
8.2	Discussion . . . . .	57
<b>9</b>	<b>Conclusion</b>	<b>59</b>
<b>10</b>	<b>Suggestions for Further Research</b>	<b>61</b>
<b>A</b>	<b>Appendix</b>	<b>I</b>

# Chapter 1

## Introduction

### 1.1 Background

Shell structures can be used to create smart, lightweight and rigid structures that have almost pure membrane action. A concept to minimise the thickness and weight is to use more lightweight material.

Reinforcement is necessary in concrete structures to increase its strength in tension. Ferrocement, which is the most common reinforcement material for shells, has been used for many decades. Further research has developed a new type of reinforcement, textile reinforced concrete (TRC), which is coated woven grids of carbon or glass fibres. There is a lot of interest in TRC, since it has a high tensile strength and can be very flexible. In contrast to TRC, ferrocement has a high thermal conductivity, it might corrode and needs more cover. Hence, adequate knowledge of material properties is essential to appropriately model the shell.

This thesis work is made in collaboration with Block Research Group at ETH Zurich (Swiss Federal Institute of Technology Zurich) and the Division of Structural Mechanics at the Faculty of Engineering LTH, Lund University.

### 1.2 Objective and Method

Three reinforcement materials for shell structures are studied: ferrocement, glass-fibre textile and carbon-fibre textile. The objective of this study is to compare the stiffness properties of ferrocement and TRC as a reinforcement material for thin concrete shells. By numerical modelling, it is possible to find a strategy to model the properties as an equivalent material based on the material properties of concrete, fibres and steel. This is done by verifying finite computational element (FE-modelling), with experimental measurements.

The FE-modelling software, Abaqus, will be used for calculating the equivalent material properties from a representative volume element (RVE) for the three reinforcement materials. Furthermore, to develop an RVE, it is important to have knowledge of the microstructure geometries and the material properties of the reinforcement and the concrete materials. The homogenised (equivalent) material properties will be determined by applying proper loading of the RVE. The RVE will further be compared to analytical simplified linear elastic models. Finally, by comparing the results achieved from numerical analysis with the obtained experimental data and by applying the equivalent materials to a thin shell, the knowledge of TRC and ferrocement for shell structures will be improved.

## 1.3 Limitations

The following limitations apply to the study presented in this master's dissertation.

- Non-linear behaviour is out of the scope.
- Only one geometry, each for the three reinforcement materials was studied.
- Long term behaviour is not studied.

## 1.4 Report Outline

<i>Ch. 1</i>	<i>Introduction</i>	Background and purpose of the thesis.
<i>Ch. 2</i>	<i>Shell Structures</i>	A historical review and theory of shell structures.
<i>Ch. 3</i>	<i>Concrete Composites</i>	Short introduction to concrete composites and their properties.
<i>Ch. 4</i>	<i>Mechanical Testing</i>	Experimental tests of concrete beams and calculations of their stiffness.
<i>Ch. 5</i>	<i>Finite Element Model</i>	Theory of finite element method and an overview of the commercial FE analysis software Abaqus.
<i>Ch. 6</i>	<i>Numerical Study of Mechanical Testing</i>	Numerical studies of the beam specimen from the experimental test set-up.
<i>Ch. 7</i>	<i>Analytical Study of Numerical Model</i>	Analytical studies of the numerical model.
<i>Ch. 8</i>	<i>Comparison of Ferrocement and TRC</i>	Comparison of the mechanical results with the numerical and analytical studies.
<i>Ch. 9</i>	<i>Conclusion</i>	Conclusions of the mechanical, numerical and analytical comparison.
<i>Ch. 10</i>	<i>Suggestions for Further Research</i>	Suggestions for further research.

## Chapter 2

# Shell Structures

Shells, membranes and spatial structures will always have a role in architecture and engineering (Adriaenssens et al., 2014). Many inspirations of structures are taken from the nature or has been designed from various types of form finding. If the major action is in the tangential direction of the shell (membrane action), shell structures resist loads very efficiently and provide eye-catching forms, which are interesting for many designers. By learning from historical structures, more knowledge of designing future building structures are gained.

### 2.1 Historical Review

The British engineer, Robert Hooke (1635-1703), was the first who published an example of structural form finding. Hooke's law of elasticity is his most known formula, but he did also invent Hooke's hanging chain. The definition of the hanging chain is a study of a catenary under its self-weight in pure tension and free of bending. Once inverted, the shape of the catenary represents an arch geometry in pure compression.

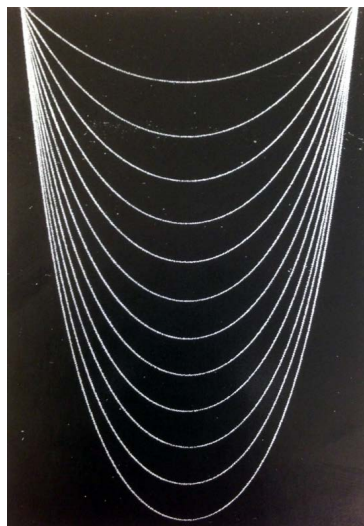


Figure 2.1: Hooke's hanging chain. Source: Otto et al. (1996).

The interest in form finding and building thin shell structures began to appear during the late 19th and early 20th century. Studying doubly curved shapes was introduced by the great architects and engineers Félix Candela Outeriño and Frei Otto. Frei Otto (1891-1979) was a structural engineer and architect from Germany who was interested in designing light and flexible buildings, in particular, tensile and membrane structures. One of his greatest works is the Multihalle (Figure 2.2), which is a grid shell in Mannheim. The structural form was derived from Frei Otto's hanging model and was built with an 80 m span, 7400 m<sup>2</sup> of roof area and with self-weight of 20 kg/m<sup>2</sup>. Today, it is one of the largest and lightest timber compression structures ever built. Furthermore, Félix Candela (1910-1997) was a brilliant architect and structural engineer from Spain. He was studying hyperbolic parabolic geometries and was designing thin concrete shells. One of the most famous is Chapel Lomas de Cuernavaca (Figure 2.2) in Mexico. The saddle shaped building has a minimum of 18 m span and 40 mm thickness.

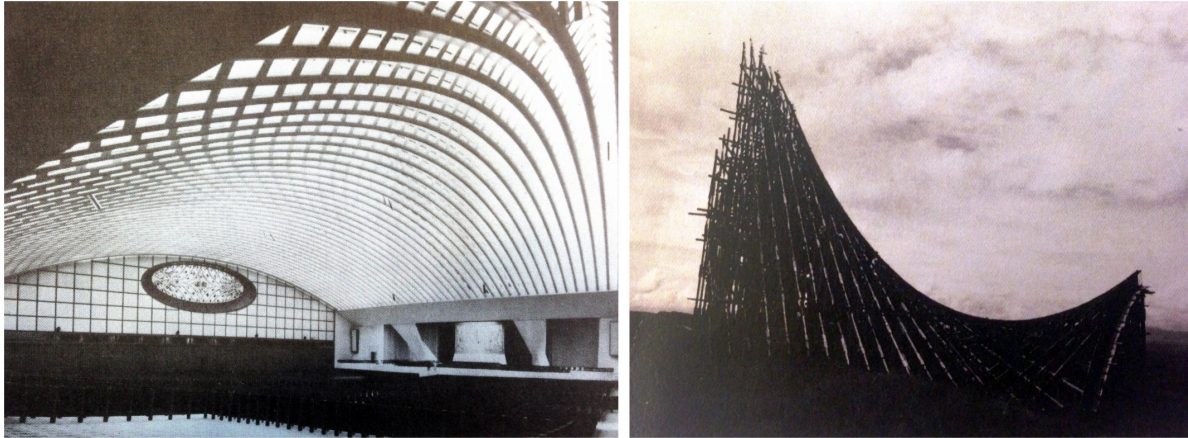


Figure 2.2: Multihalle in Mannheim by Frei Otto to the left and formwork of Chapel Lomas de Cuernavaca by Félix Candela to the right. Source: To the left Otto et al. (1996) and to the right photo by Eduardo Alarcón.

These structures have become less attractive with the declining price of steel and a rising cost of labour. As a consequence, researchers are trying to find other ways to recreate those historical buildings. Research in form finding, flexible formwork and new materials for shell structures, such as ferrocement and TRC, is just on the doorstep of real technological evolution (Block Research Group).

## 2.2 Current Projects

The experiments, presented in this thesis work, are intended to give further ideas and inform the design of the HiLo roof in Dubendorf, Switzerland, as shown in Figure 2.3. HiLo is a duplex penthouse apartment on top of the NEST building, which consist of a doubly curved concrete roof. The research and innovation building NEST is a five storey building centre of Empa and Eawag in collaboration with the ETH Domain. NEST consist of multiple units – where HiLo is one of them – which will give the opportunity to test innovative ideas, having workshops, student housing and conferences. For each of these units, there is an independent design team consisting of commercial parties such as engineers, architects and at least one academic partner ([www.block.arch.ethz.ch](http://www.block.arch.ethz.ch)). NEST HiLo will be built on the Empa campus outside Zurich in Dubendorf, due to be completed in 2015/2016.

## 2.3 Structure of a Shell

Shells can be classified in many ways dependent on their structure, function and material. There are no rules for how thin a shell should be. The common definition of a shell is a double curved surface, which is thin in the direction perpendicular to the surface.

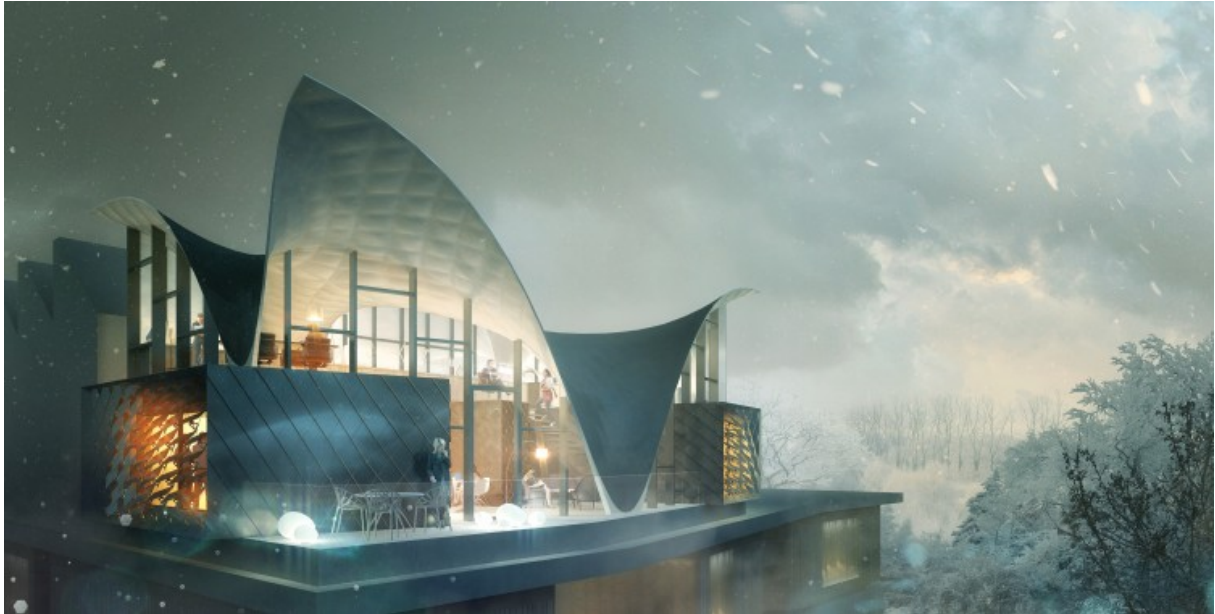


Figure 2.3: NEST HiLo in Dubendorf, outside Zurich. Source: Block Research Group.

A surface that only has a negative Gaussian curvature is called anticlastic, such as the roof of NEST HiLo. In comparison, the two directions are called synclastic, which have the shape as a cooling tower and has a positive Gaussian curvature.

There are many applications and objects where it is possible to put the definition of the word, shell. This thesis work, only includes the definitions of shells in a structural manner. In addition, there are many approaches to understanding shells. Plates are much easier to understand than shells, so let us start with them first and then end up with the membrane theory of shells.

### 2.3.1 Plate Theory

In all kind of situations, stresses are appearing during loading. It is clear, when a beam is axial loaded, stresses are acting in the web and flanges. Those stresses are called in-plane stresses. Structures that are loaded out of plane creates plate bending. Bending a plate is much easier than to stretch it, for instance in-plane loaded structures.

Understanding in-plane stresses for plates is a central part in understanding shell theory. Figure 2.4 shows normal stresses,  $\sigma_x$ ,  $\sigma_y$  and  $\sigma_z$ . These stresses are called the membrane stresses and occur in all three axial directions. The shear stresses,  $\tau_{xy}$ ,  $\tau_{yx}$ , etc., occurs perpendicular to the axial directions. Note that the membrane stresses are usually described as a force per unit length, not per unit area.

All forces that are acting on the plate are illustrated in Figure 2.5. The shear stresses are acting in the plane of the plate and perpendicular to it. There are three unknown stresses and only two known equations (2.1) and (2.2). In order to find a solution for them, the stresses can be written as the Airy stress function, such as (2.3), (2.4) and (2.5) if the loads  $q_x$  and  $q_y$  both are zero (Adriaenssens et al., 2014).

$$\frac{\partial \sigma_x}{\partial x} + \frac{\partial \sigma_{yx}}{\partial y} = q_x \quad (2.1)$$

$$\frac{\partial \tau_{xy}}{\partial x} + \frac{\partial \sigma_y}{\partial y} = q_y \quad (2.2)$$

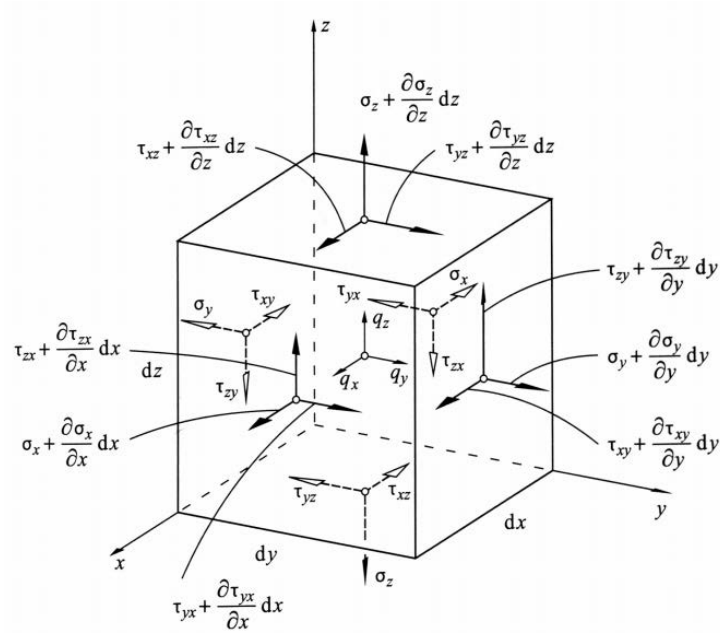


Figure 2.4: Plane stress. Source: Marti (2012).

$$\sigma_x = \frac{\partial^2 \phi}{\partial y^2} \quad (2.3)$$

$$\sigma_y = \frac{\partial^2 \phi}{\partial x^2} \quad (2.4)$$

$$\tau_{xy} = \tau_{yx} = -\frac{\partial^2 \phi}{\partial x \partial y} \quad (2.5)$$

It is possible to solve  $\phi$  if the plate is elastic by using the expressions (2.6), (2.7) and (2.8).

$$\varepsilon_x = \frac{1}{E}(\sigma_x - \nu \sigma_y) \quad (2.6)$$

$$\varepsilon_y = \frac{1}{E}(\sigma_y - \nu \sigma_x) \quad (2.7)$$

$$\gamma_{xy} = \frac{2(1+\nu)}{E} \tau_{xy} \quad (2.8)$$

The  $E$  is Young's modulus and  $\nu$  is Poisson's ratio, which gives the compatibility equation,

$$\frac{\partial^2 \varepsilon_x}{\partial y^2} - \frac{\partial^2 \gamma_{xy}}{\partial x \partial y} + \frac{\partial^2 \varepsilon_y}{\partial x^2} = 0. \quad (2.9)$$

This leads finally to the differential equation,

$$\nabla \nabla \phi = \frac{\partial^4 \phi}{\partial x^4} + 2 \frac{\partial^4 \phi}{\partial x^2 \partial y^2} + \frac{\partial^4 \phi}{\partial y^4} = 0 \quad (2.10)$$

which is known as the biharmonic equation.

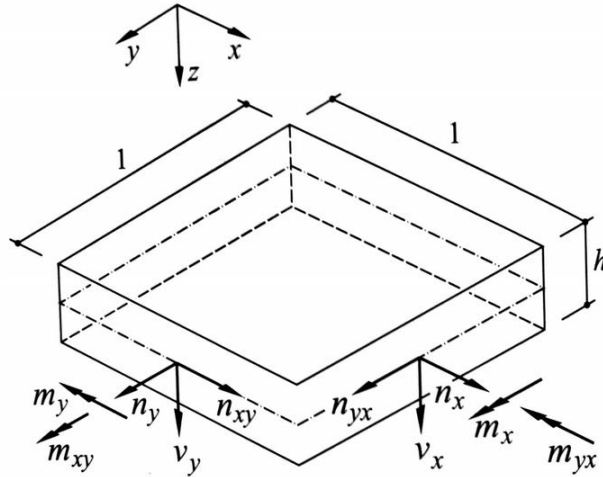


Figure 2.5: Plate bending. Source: Marti (2012).

### 2.3.2 Membrane Theory

The membrane theory has similarity with the case of plane stress since there are three components of membrane stress. However, the bending moments and the shear forces are neglected due to the thickness of the shell (Vogel, 2012).

In membrane theory, it is difficult to find approximate solutions for a shell. Hence, there are three partial differential equations of equilibrium in three membrane stresses. The differential equations depend on the boundary conditions and the shape of the shell. There are three equations of equilibrium that describes the forces acting on the shell. One which is perpendicular to the surface and the other two which are in the direction of the shell surface, as been shown in Figure 2.6. The system is statically determined since there are three unknown stresses and three equations (Adriaenssens et al., 2014).

The radius of curvature in the  $x$ -direction is  $r_1$ . In  $y$ -direction, the radius of curvature is  $r_2$  and the  $z$ -axis is perpendicular to the middle surface. Similarly as in the plate theory, the load consist of in-plane forces  $q_x$ ,  $q_y$  and out-of-plane forces  $q_z$ , in the  $x$ ,  $y$  and  $z$ -directions respectively. Furthermore, the displacements  $u_x$ ,  $u_y$  and  $u_z$  occur together with the normal stresses  $\sigma_x$ ,  $\sigma_y$  and  $\sigma_z$ . These normal stresses are uniformly distributed through the thickness and integrate to  $n_x$ ,  $n_y$  and  $n_{xy}$ . However, the shear membrane force  $n_{xy}$  is equal to  $n_{yx}$  due to the moment equilibrium condition with respect to the normal axis in  $z$ -direction (Blaauwendraad and Hoefakker, 2014).

The easiest way to do this more understandable is to use plane coordinates. If the shell is loaded only in the vertical direction, the horizontal equilibrium equations in (2.1) and (2.2) are still satisfied by use of the Airy stress function. The equilibrium in the vertical direction will then be

$$w = \frac{\partial^2 \phi}{\partial x^2} \frac{\partial^2 z}{\partial y^2} - 2 \frac{\partial^2 \phi}{\partial x \partial y} \frac{\partial^2 z}{\partial x \partial y} + \frac{\partial^2 \phi}{\partial y^2} \frac{\partial^2 z}{\partial x^2} \quad (2.11)$$

where  $x$  and  $y$  are functions,  $\phi(x, y)$ ,  $z$  is the height of the shell and  $w$  is the load per unit area. Even if the function (2.11) does not look much more complicated than the biharmonic equation (2.10), the function may undergo inextensional deformation due to the bending of the shell without stretching. Hence, it is significant to have the right boundary conditions and right shape of the shell (Adriaenssens et al., 2014).

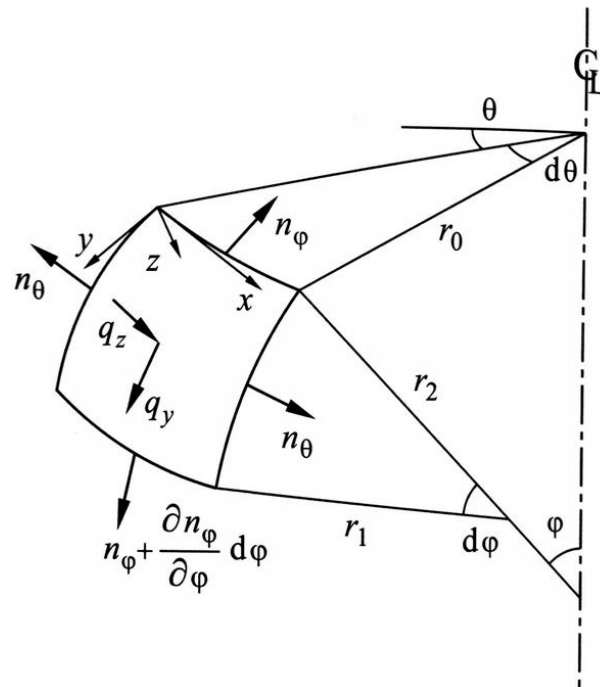


Figure 2.6: Membrane forces in a shell. Source: Adriaenssens et al. (2014).

# Chapter 3

## Concrete Composites

Concrete is a material which has high strength in compression. Its strength in tension is, though, much lower. Hence, the reinforcing material, steel, has been a common material to increase the strength in tension. Despite this, TRC has opened other possibilities in this manner.

This chapter will give an introduction to reinforcing materials and discuss their properties, strength and composition. The chapter will end up with a section about comparing ferrocement and TRC for concrete applications.

### 3.1 Concrete

Nowadays, there are three commonly used structural materials: concrete, steel and timber. The composite material, concrete, consists of mainly water, aggregate, cement and reinforcement. Concrete is a common building material and is appropriate for structures, such as bridges or dams, highways or buildings.

#### 3.1.1 Definition

The concrete is a material of the reaction between hydraulic cement and water. In other words, cement is to concrete what flour is to a cake, and the quality of the cake depends on the quality of the ingredients and the cook. In addition, concrete mixes could contain a wide range of mixture products. For instance, pozzolan, fly ash, blast-furnace slag, micro-silica, additives, recycled concrete aggregate, admixtures, polymers and fibres. The concrete materials could further be heated, steam-cured, autoclaved, vacuum-treated, hydraulically pressured, shock-vibrated, extruded and sprayed (Neville and Brooks, 2010). The manufacturing process guarantees the quality of the concrete.

#### 3.1.2 Composition

The composition of concrete depends much on the area of application, such as if the concrete will be used in a bridge or as a structural element for a high building.

Commitments concerning the strength and durability are dependent on the additives, texture and the strength. The quality of the main ingredients, cement, aggregates and water, will also have a great influence on the concrete properties. These three components will be discussed in the following sections.



Figure 3.1: Submarino Restaurant by Félix Candela in Valencia, Spain. Source: Hertzell et al. (2003).

### 3.1.2.1 Cement

The ancient Romans were probably the first to use concrete, which was based on hydraulic cement and water. The Roman cement fell into disuse and became later in 19th century patented and known as Portland cement, by the builder Joseph Aspdin.

The definition of Portland cement is a mix of calcareous and argillaceous, or other silica-, alumina, and iron oxide-bearing materials burning and grinding them at a sufficient temperature. However, a British, European or American Standard definition of cement can be viewed as a combination of the calcareous materials, limestone and chalk with the clay and shale materials, silica and alumina. The manufacturing of cement consists of three steps. Firstly, the raw materials have to be grinded into a fine powder. Secondly, the powder must be mixed and burned in a large rotary kiln at very high temperatures, up to 1400°C. Now, the material will sinter and fuse into clinker. The third and last step, some gypsum is added to the cooled clinker, which results in a complete cement product (Neville and Brooks, 2010).

The grinding and mixing of the raw materials can be done either in water or dry condition, hence the names wet and dry process. First, when the mixture moves down the kiln, the temperature rises and the chemical compounds vary along the kiln. During this stage, the water is driven off and CO<sub>2</sub> is released from the calcium carbonate. The dry material passes many reaction series until it reaches the hottest part of the kiln, where some 20-30% of the material becomes liquid, where lime, silica and alumina recombine into clinker. After a while, the cooling process of the clinker starts. However, the rate of the cooling gives the cement material its degree of crystallisation. The cool clinker, which now is very hard, is interground with gypsum to prevent flash-setting (Neville and Brooks, 2010). The ground material is cement, which is the final product.

### 3.1.2.2 Normal Aggregate

The concrete volume consists roughly of three-quarters of aggregate since the aggregate quality is of considerable importance for the properties of the concrete. Aggregate is not a concrete material as to produce a large volume of the concrete mass. Instead, its physical, thermal and chemical properties are of interest since those properties influence much more than previously believed.

Aggregates can be formed by natural weathering or by artificially crushing a larger parent mass. Properties of the aggregate such as chemical and mineral composition, petrographic classification, specific gravity, hardness, strength, physical and chemical stability, pore structure and colour depend on the properties of the parent rock. In addition, there are properties of the aggregate that are absent in the parent rock: particle shape and size, surface texture and absorption. All these properties may influence considerably on the quality of fresh and hardened concrete (Neville and Brooks, 2010).

There are a range of aggregate sizes for concrete, particles from 10 mm up to 50 mm is common. The size of a particle is called grading. Sometimes the term for aggregates is meant to be a coarse aggregate in contrast to the sand. The truth is that there could be much lower particle grades for concrete, called fine aggregate (Neville and Brooks, 2010). Sand is a fine aggregate and has a limited size of about 0.007 mm or less. The sand material, as silt, is defined as 0.02-0.06 mm and smaller particles than that are called clay.

In particular, the surface texture and the particle shape are of great importance regarding the properties of fresh and hardened concrete. It is difficult to describe the shape of a three-dimensional body, especially bodies such as aggregates. In order to make it easier to compare good with bad aggregates, there is a standard system where it is possible to measure roundness, sphericity and surface texture.

### 3.1.2.3 Quality of Water

As a rule, many specifications for concrete mixing says that the water should be fit for drinking. Also, the water shall not taste brackish or saline and the pH should be between 6.0-8.0, in order to satisfy the degree of acidity. Moreover, water that contain organic material may adversely affect the hardening concrete. As a matter of fact, a dark colour or a bad smell do not necessarily mean that the water is useless. Despite this, bad water quality may cause an adverse effect on the strength of the concrete or cause staining of its surface. In addition, it may also lead to corrosion of the reinforcement (Neville and Brooks, 2010). It is obvious that the water affects the quality of the final concrete.

## 3.1.3 Physical Properties

### 3.1.3.1 Density

Density  $\rho$  is defined by the ratio between mass and volume. The general and most common used density in concrete engineering is approximately 2400 kg/m<sup>3</sup>. The density is divided into two definitions of density: particle density and bulk density. The particle density of concrete is the "true density" of material (2300-2400 kg/m<sup>3</sup>) and is not dependent on the compaction of the material. In contrast, the bulk density (dry density) for concrete is when the material is compacted. The bulk density can change depend on the shape of the particles or on how the material is handled and packed. There is also a third, fresh density, which is the density when the concrete is unhardened and still wet.

### 3.1.3.2 Porosity

The pores vary in size over a wide range. The water can penetrate inside the pores and by hydration take three forms: combined water, gel water and capillary water.

The gel water is the water that is located between the products of hydration in so-called gel pores. The gel pores are approximately 2 nm in diameter, which is very small pores. Furthermore, the capillary pores are as well included in the total pore volume. They represent 23% of the total dry cement mass, in a fully hydrated state. Gel pores are much smaller than capillary pores (Neville and Brooks, 2010).

The total cement porosity,  $p_t$ , is defined as,

$$p_t = \frac{\frac{W}{C} - 0.17h_w}{0.317 + \frac{W}{C}} \quad (3.1)$$

where  $h_w$  is the degree of hydration and  $\frac{W}{C}$  in (3.1) is the relation between water and cement. The porosity of concrete influences the bond, resistance to freezing and as well as the strength.

### 3.1.3.3 Microcracking

It has been verified that very small bond cracks exist at the interface between the coarse aggregate and hydrated cement paste. They are called microcracks and occurs as a result of differential volume changes, which could be changes in temperature, moisture or differences in stress-strain behaviour. Figure 3.2 shows that the stress-strain relations for the aggregate and the cement paste have a linear behaviour (Neville and Brooks, 2010). However, for concrete, the stress-strain relation becomes curvilinear at higher stresses.

## 3.1.4 Mechanical Properties

There are several common properties of concrete, e.g. strength and stiffness. All of them are dependent on the characteristics of concrete as already mentioned.

### 3.1.4.1 Strength

Many times, strength, as well as durability and volume changes of hardened cement paste, are not dependent on the chemical composition as on the physical structure of the cement hydration and volumetric proportions. In particular, the porosity of the hydrated cement and microcracking are the factors that are pertinent to consider the mechanics of fracture of concrete under stress (Neville and Brooks, 2010). However, the porosity and the microcracking are factors that are difficult to assess. These factors can be seen as sources of weakness.

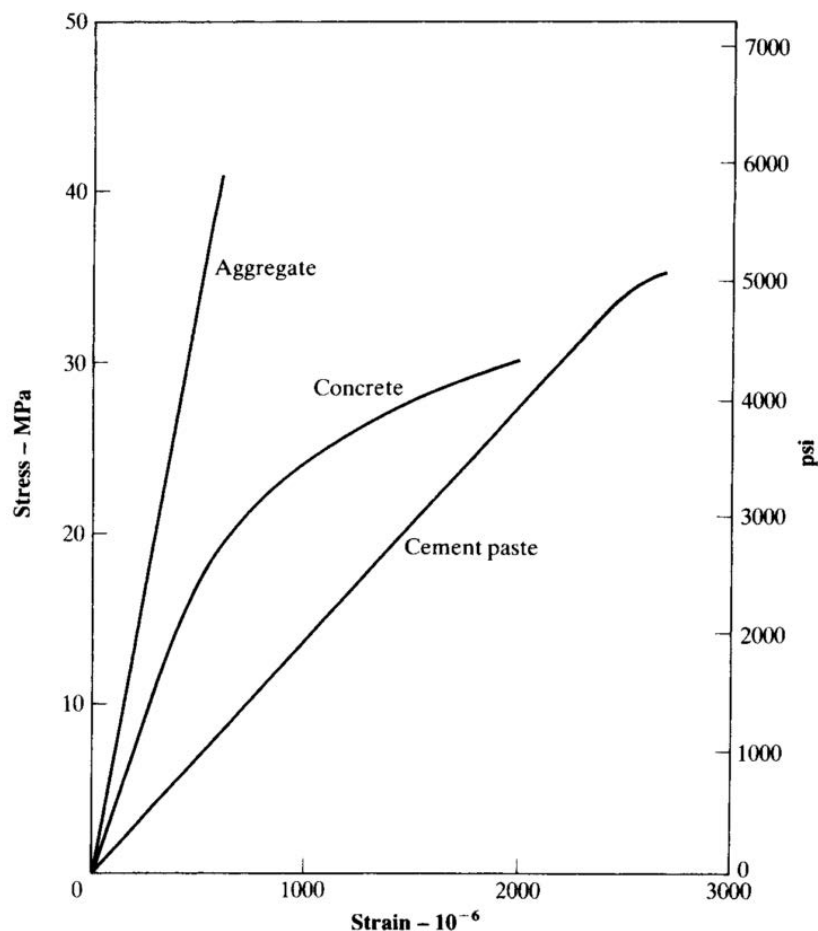


Figure 3.2: Stress-strain relation for cement, aggregate and concrete. Source: Neville and Brooks (2010).

In addition, the bond of concrete will also play a role for the strength. The size, texture and surface area of the aggregate may change the adhesion between the aggregate and the cement matrix. This will, as a result, affect the bonding forces between the cement particles and the aggregate. All these characteristic factors have a great influence on the concrete strength.

### 3.1.4.2 Stiffness

The Young's modulus,  $E$ , is the stiffness of isotropic concrete and depend mostly on the properties of the aggregate. The stiffness is increasing with higher compression strength. The relationship between the Young's modulus and the compression strength of concrete is given in Equation 3.2, where the  $f_{cm}$  is the mean compression strength (Engström, 2006).

$$E_{cm} = 22 \left( \frac{f_{cm}}{10} \right)^{0.5} \quad (3.2)$$

Poisson's ratio is  $\nu = 0.2$  for normal concrete.

## 3.2 Ferrocement

### 3.2.1 Definition

Ferrocement is a form of reinforced concrete that differs from the traditional reinforcement composition in concrete. In contrast to the conventional reinforcement technique, the elements of ferrocement are primarily dispersed and arranged. The most common reinforcement material in ferrocement is steel. Yet, there are characteristics of ferrocement that can be achieved with reinforcement other than steel meshes or rods. In spite of this, research has been made using other materials for meshes. Alkali resistant glass and organic woven fabrics, such as burlap and bamboo fibres, are materials that have been tested. The definition of ferrocement adopted by the Committee of American Concrete Institute (ACI), published in 1980 and still enforced:

*"Ferrocement is a type of thin wall reinforced concrete commonly constructed of hydraulic cement mortar reinforced with closely spaced layers of continuous and relatively small size wire mesh. The mesh may be made of metallic or other suitable materials."*

### 3.2.2 Composition

The ferrocement is a composite material and consist of reinforcement embedded in cement mortar. The reinforcement material is usually a mesh, which is fabricated from single strand filaments. The mesh structure can have a different look, dependent on how they are woven. They can either be woven or interlocking (hexagonal, such as chicken wire cloth), woven cloth mesh in with filaments are interwoven, welded and finally woven patterns that may include diagonal filament woven through the rectangular mesh pattern. However, hexagonal meshes are not structurally efficient as meshes with square openings because the wires are not always oriented in the direction of the maximum stresses (Arockiasamy et al., 2009). Note that the mesh wire does not need to have a small size wire mesh, since ferrocement can also comprise skeletal steel reinforcement of larger diameter. Some examples of different meshes are illustrated in Figure 3.3 (Naaman, 2012).

Furthermore, the matrix consists primarily of hydraulic Portland cement and works as an inert filler material for ferrocement. The gravel size of the aggregate depends on the opening and the distribution of the mesh. However, the matrix represents approximately 95% of the ferrocement volume. Hence, the physical properties of the cement have a great influence of the final product (Arockiasamy et al., 2009).

In summary, there is a variety of mesh dimensions and matrix compounds. Properties of the final ferrocement can be affected by the filament size, wire strength, ductility and how well the mortar matrix penetrates the reinforcement mesh (Arockiasamy et al., 2009).

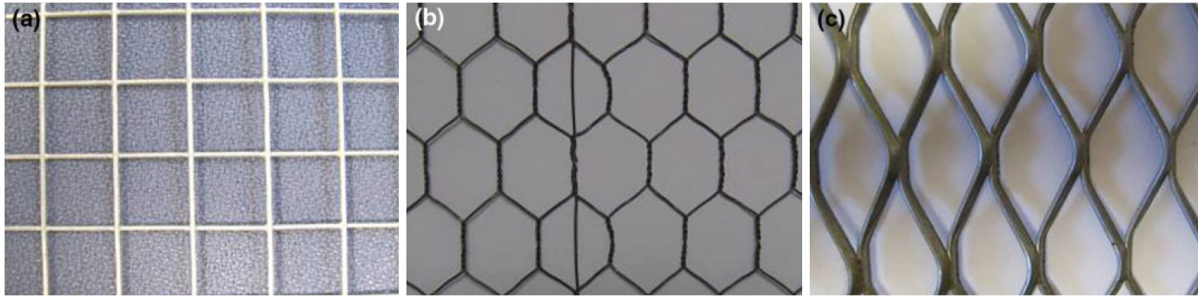


Figure 3.3: Conventional steel meshes used in ferrocement. Figure (a) shows a square woven or welded mesh. Hexagonal or chicken wire mesh (b) and expanded metal lath (c), Naaman (2012).

### 3.2.3 Physical Properties

The orientation, the volume fraction and the effective area of the reinforcement influence on how much stress it is possible to introduce to the reinforcement mesh. The orientation is defined as the angle in degrees between the reinforcing elements and the direction of the applied stress. For instance, the effective area of steel in a particular direction is based on the cross-sectional area of the elements multiplied by the cosine of the angle between the elements and the direction of the applied stress. As shown in (3.3) (Arockiasamy et al., 2009).

$$A_{ef} = A \cos \alpha \tag{3.3}$$

Physically, it is difficult to put more than 8% of steel in ferrocement. Generally, the total volume of ferrocement ranges from about 2-8%. A value of 8% is typically obtained by packing together as many layers of mesh as possible within the composite. As a result, both the tensile and bending resistance of the composite increase with the volume fraction of reinforcement (Naaman, 2012).

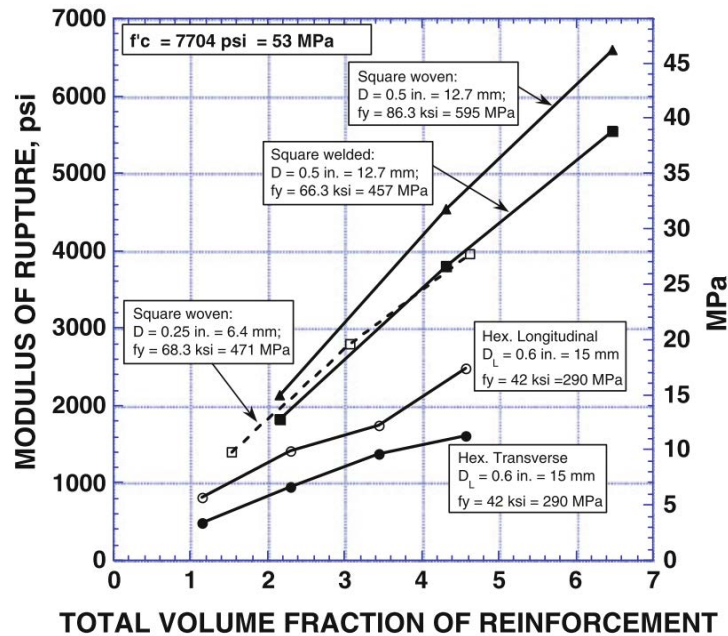


Figure 3.4: Modulus of rupture of ferrocement plates versus volume fraction of reinforcement using conventional steel wire meshes. Source: Naaman (2012).

### 3.2.4 Mechanical Properties

Ferrocement is regarded as a homogenous-orthotropic material, even if it is reinforced in two directions. It has a high tensile strength and a high modulus of rupture. Compared with conventional reinforced concrete, bonding forces between the steel and the matrix are much larger for ferrocement.

### 3.2.5 Applications

The idea to use closely spaced layers of fine wire mesh surrounded by mortar matrix was originally conceived by Joseph-Louis Lambot (1814-1887) for concrete boat building. His concept was subsequently resurrected by the Italian engineer Pier Luigi Nervi (1891-1979). He is known as a well-respected structural engineer and was one of the first who demonstrated the utility of ferrocement for structures. Since then, ferrocement has been studied as a material for design and construction applications (Naaman, 2012).

Ferrocement does not need any high technical skills. It even does not require heavy machinery or plants, which make the material suitable for rural applications in developing countries. However, in urban areas the potential purpose of ferrocement must be viewed from another perspective. Since the tensile strength to weight ratio is high, the material is ideally suited for thin wall panels, roofs, tanks and boats (Arockiasamy et al., 2009).



Figure 3.5: Left side, curtain wall construction the Institute of Structural Concrete, RWTH Aachen, Grosse (2007). Right side, ferrocement tank for rainwater collection, Arockiasamy et al. (2009).

#### 3.2.5.1 Boats, Tanks, Silos and Roofs

Many countries have used ferrocement as a building material for boats. The country that has introduced large-scale productions by ferrocement is China. Other countries have only used ferrocement in a small production amount of the total boat industry.

Furthermore, villages in most developing countries are using ferrocement for storage facilities. Up to 25% of the rice is lost due to vermin populations such as birds, fungi and insects. The ferrocement silos and tanks can accommodate up to 30 tonnes of grain and  $46 \text{ m}^3$  of water, which is a quite good economical solution for developing countries.

There is an urgent need for finding economical material for building roofs since the material costs are very high for roofs compare to other construction elements. Therefore, it seems that ferrocement can be a good economical alternative and as well an interesting material for researchers (Arockiasamy et al., 2009).

### 3.3 Textile Reinforced Concrete

There is a great amount of materials that can be divided into four classes: metals, polymers, ceramics and composites. Fibre and textile reinforced materials are a part of the general class called composites. Textile reinforced materials have had a low-profile in many years until it became more interesting for researchers to use textile reinforced material as an alternative to current reinforcing materials. The use of modern building lightweight materials gives designers and architects the opportunity to create more slender and eye-catching structures.

#### 3.3.1 Definition

Textile reinforcement concrete (TRC) is a composite material, which consist of a fine-grained concrete matrix and reinforcement fibres. The fibres are applied as fibre bundles. The bundles are called multi-filament yarns and consist of several hundred elementary fibres called filaments. The structure of a TRC have a two or three-dimensional orientation and behaves like normal steel reinforcement (Hartig et al., 2012). Compared to steel reinforcement such as ferrocement, TRC is lighter and more flexible and is therefore much easier to construct with.

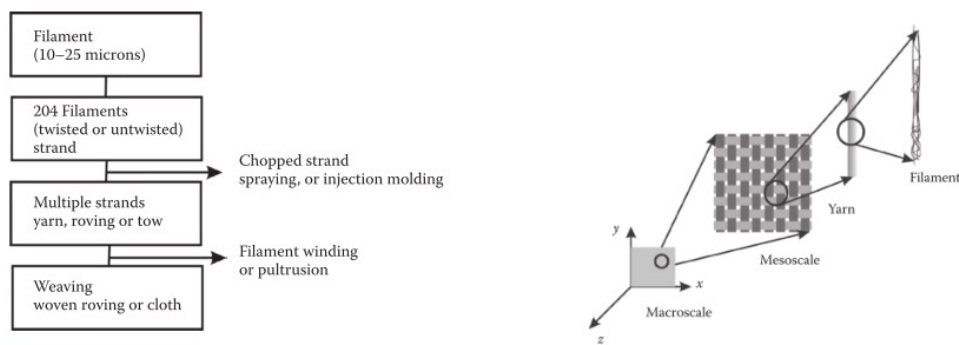


Figure 3.6: TRC from macro to a micro scale. Source: Mobasher (2011).

#### 3.3.2 Composition

There is a large range of fibre and matrix combinations available for textile reinforced composites. Also, there are a wide number of manufacturing possibilities in arranging fibres. The most common filament yarns used in TRC is AR-glass and carbon. Their high tensile strength and their good resistance to corrosion make them to a good choice as a reinforcing material.

##### 3.3.2.1 Glass

It is clear that the glass material, E-glass (as used by the FRP industry) was a chemically unstable material in high alkali environments, such as concrete. Further development of the glass industry could bring new alkali resistant AR-glass, which is much more durable in concrete applications.

The development of AR-glass started in the 1970s by Pilkington. AR-glass is based on the silica-soda-calcia glass with approximately 16% zirconia. The production of glass occurs at temperatures up to 1350°C, where the fibres are spinned in diameters ranging from 9 to 27  $\mu\text{m}$ . The density is 2800  $\text{kg}/\text{m}^3$  and the tensile strength can be up to 1400 MPa with a Young's modulus of 70-80 GPa (Gries et al., 1998).

### 3.3.2.2 Carbon

Thomas Alva Edison was the first pioneer using carbon fibres for electric light bulbs. However, the development of carbon fibres started in the 1960s. Today the carbon fibres are used as a high strength material for the aviation, automobile and sports industry.

The materials that are used are polyacrylnitrile and meso pitch, which can be made spinnable by polymerisation or thermal treatment (Gries et al., 1998). The carbonisation stage defines the properties of the carbon fibres. The common tensile strength of carbon fibres is about 3000-5000 MPa and the Young's modulus about 200-250 GPa.

The advantages of carbon fibres regarding the material properties are e.g. the low density ( $1800 \text{ kg/m}^3$ ), very little creeping, low conductivity, good electric conductivity and high resistance to acid, alkaline and organic solvents. However, despite its good material properties the adhesion to concrete is not as good as that of AR-glass. The high cost is another factor. Having solved this problem carbon will have an increasing importance in reinforcing concrete (Gries et al., 1998).

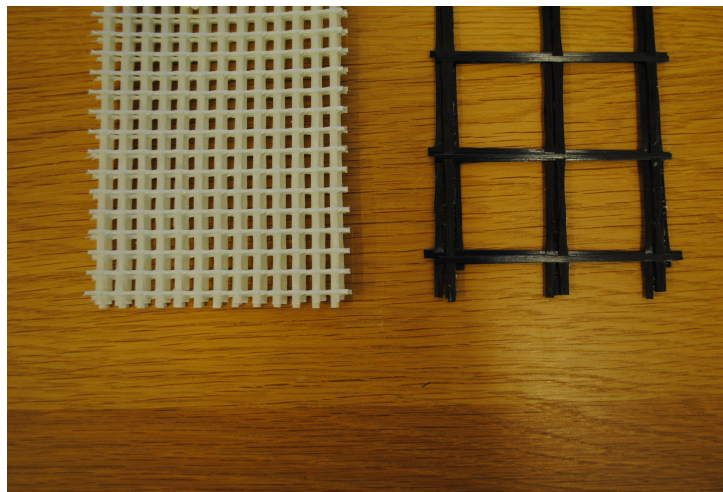


Figure 3.7: Glass (left) and carbon reinforcement (right).

### 3.3.2.3 Construction

The properties, the amount and the arrangement of the fibre materials have a great influence on the mechanical behaviour of TRC. TRC fabrics have different structures, depend on how they are woven. Manufacturing processes include methods such as hand layup, autoclave, resin transfer moulding, squeeze casting and chemical vapour infiltration.

The textile forms consist of small filaments, which are called strands for glass fibres and tows for carbon fibres. A larger group of strands or tows are called rovings. In order to manufacture fine textile fabrics, the filaments can be twisted into yarns, which is illustrated in Figure 3.6. Finally, to produce a woven textile fabric there are many warping techniques. One of the techniques are scrims, warp knits and woven fabrics (Mobasher, 2011).

There are three basic weaving arrangements: plain, twill and satin. The plain weave has the shortest floating and a very high displacement stability (Gries et al., 1998). Also, it is warped over and under one filling yarn. Compare to the plain weave, the twill weave is thread over and under two or more filling yarns. Furthermore, the satin weave interlocks over three to seven yarns, which gives the highest strength composite, see Figure 3.8.

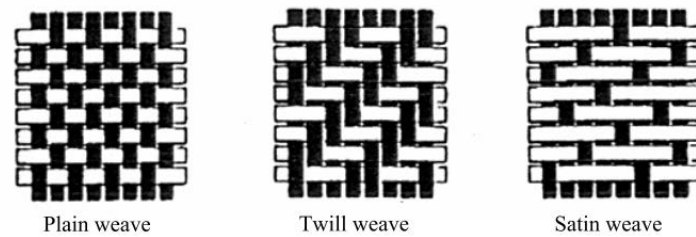


Figure 3.8: Weaving arrangements. Source: Gries et al. (1998).

### 3.3.3 Physical Properties of TRC

#### 3.3.3.1 Durability

TRC has a great resistance to corrosion, which is one of the greatest advantages in durability. The durability of TRC is very complicated since many variables have to be taken into account. For instance, the bonding behaviour between the carbon fibres and the concrete matrix is conditioned by the chemical treatment of the fibres. It is significant which cement is used and how its behaviour is in time (Petre and Zapalowicz, 2012).

#### 3.3.3.2 Bonding Behaviour

It is of significance to understand the interaction between the textile fibres and the concrete matrix in order to understand the behaviour of the material during loading. The effect of the bonding between the reinforcement for the textile and the concrete can be described by a bond-slip diagram (Petre and Zapalowicz, 2012).

### 3.3.4 Mechanical Properties of TRC

Compared to traditional reinforcement materials, TRC has a high load carrying capacity. The expected load capacity of the textile is dependent on the material, the properties of the textile and the penetration depth of the matrix (Hartig and Jesse, 2010).

The choice of TRC depends on the expected loading. The matrix does not penetrate the fibre bundles completely due to the size of the aggregate. The loads are transferred by direct contact with the concrete to the outer sleeve fibres and further to the inner core fibres. That creates stresses in the material. If the maximum strength of a fibre is achieved, slip occurs. This failure could finally lead to a non-uniform stress and strain relationship in the filaments. The stress and strain relationship depend on, e.g. bond strength, fibre bundle geometry and fibre stiffness (Hartig and Jesse, 2010).

When the concrete cracks under tensile loading, the textile fibres must withstand the tension forces to prevent crack failure. The critical fibre volume is the amount of fibres that is required to resist the cracking load.

### 3.3.5 Applications of TRC

TRC covers large areas of applications. The textile reinforcement could be used in existing structures for strengthening and for new structure purposes. Nowadays, TRC is used for strengthening structural elements. For instance beams, bridges, floors and roofs. Even non-bearing elements could be constructed by TRC to resist flexural loading (Petre and Zapalowicz, 2012).

### 3.4 Comparison between Ferrocement and TRC

The field of composite materials, through appealing inventions and analysis, provides many opportunities still. The concrete properties of composite compound are determined by the material properties of its constituents. The ambition here is to discuss the comparison between ferrocement and TRC.

Firstly, TRC, particularly carbon-fibre TRC, can carry high tensile loads and is also much lighter than ferrocement. Secondly, in this study, ferrocement have a greater effective area than the carbon and glass textiles. Thirdly, the protection against corrosion is better for the glass and carbon textiles than for ferrocement. However, there is a fourth that is important, the textile composites are more flexible than the ferrocement, which makes the textiles easier to construct.

Ferrocement was used in a larger range during the turn of the 19th and 20th century. Today, it is unknown what possibilities the material can bring the building industry to and in which new applications it can be used. With modern material technology, woven textile reinforcement material is becoming a more attractive choice for the architect and give the engineer more freedom in design. A deeper understanding of the composite materials is of a great significance. Hence, thinner and lighter shell structures can be created.



# Chapter 4

## Mechanical Testing

Experimental tests were performed at the concrete laboratory at the Division of Building Materials at LTH. The purpose was to investigate the stiffness properties of concrete beams by a four-point bending test with glass and carbon textile reinforcement and with woven steel reinforcement.

This chapter will explain the experimental program, from the preparation of the composition to the bending tests of beams. Results are presented and discussions are made regarding the conclusions from the experiments.

### 4.1 Experimental Program

The stiffness properties of nine composite beams were determined by a four-point bending test, since the stiffness strength is directly related to the maximum stress of the beam. The stress volume, between the two axial loads, of a four-point bending test is greater than the volume under a three-point bending. This will contribute to a more accurate strength value in this area. Hence, the answer will be more relevant from a statical point of view. The beam set-up was defined as a simply supported beam with two loads and a total load  $P$ . The experiment was carried out in a testing machine.

$$P = 2F \tag{4.1}$$

The beam specimens had an effective span of 700 mm, and the loads were applied 200 mm from the supports. The loads were applied to steel plates where a roll and fix support was laying on top of the plates. The span was 300 mm between the plates, see Figure 4.1.

This set-up was also studied by numerical and analytical investigations. Using Equation 4.2, stiffness could be determined for the mechanical, numerical and analytical study. Figure 4.1 shows how the beam set-up is determined for the three test studies. In the following sections, the experimental programme will be explained.

$$k = \frac{P}{\delta} \tag{4.2}$$

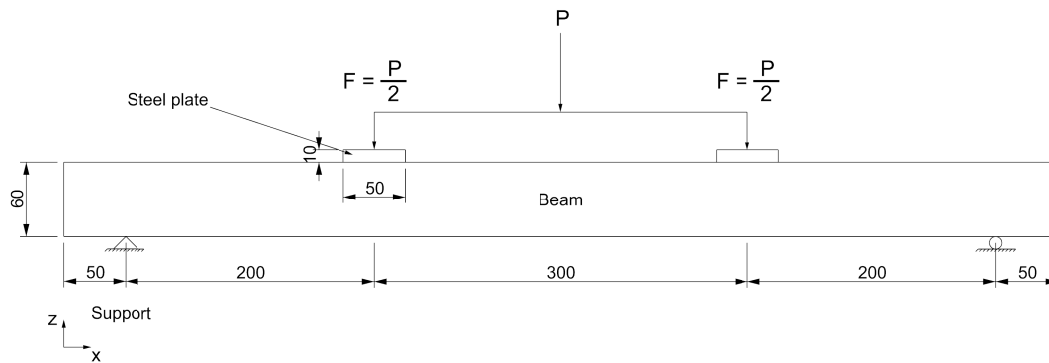


Figure 4.1: The model set-up.

#### 4.1.1 Preparation of Test

The used reinforcement materials for the mechanical experiment were glass and carbon textile, Sto Pansarväv and StoFRP Grid respectively. Furthermore, there was no technical specification for the woven steel reinforcement, since it was based on the availability of materials in the concrete laboratory. The wire mesh was an ordinary galvanised wire mesh for building façades with the mesh dimensions 10 mm x 10 mm, which was a sufficient size in this research. For this reason, comparable relative values were used from Naaman (2000). Finally, the dimensions for the glass and carbon textiles were 7.5 mm x 7.5 mm for glass and 38 mm x 38 mm for the carbon textile fabric.

However, the mix design was not the interesting part and the focus of this study. Instead, the criteria was to achieve a mixture with a high strength and with a sufficient aggregate size. If the strength value is sufficiently high the stiffness would be appropriate. In the same manner for the aggregate size. The size of the aggregate particles has to be smaller than the mesh size of the reinforcement in order to sufficiently penetrate the reinforcement meshes. Due to these reasons, a Weber exm 721 expanded concrete super with a high compression class of C72/90 was suitable, see Table 4.3.

Table 4.1: Tensile strength for the glass and carbon reinforcement products from Sto.

	$f_t$	
Sto Pansarväv <sup>1)</sup>	>2000	N/50 mm
StoFRP Grid	5500	N/fibre yarn

1) After 28 days hardening.

Table 4.2: Stiffness properties for steel, glass and carbon.

	$E$ [GPa]	$f_{ty}$ [MPa]	$f_{tu}$ [MPa]
Steel	200	450	-
Glass	75	-	414
Carbon	242	-	753

where

$E$  Young's modulus  
 $f_{ty}$  yield tensile strength  
 $f_{tu}$  ultimate strength

Table 4.3: Specification from the manufacturer of the Weber exm 721 expanded concrete super.

Properties	Time		Notation
Mixture		13 l concrete/25 kg bag	thickness 30-300 mm
Water content		2.75 l water/25 kg bag	
Aggregate size		0-4 mm	
Water-cement ratio		0.3	
Fresh density	5 min	2410 kg/m <sup>3</sup>	Pr EN 1015-6
	30 min	2360 kg/m <sup>3</sup>	Pr EN 1015-6
Dry density		2320 kg/m <sup>3</sup>	Pr EN 1015-10
Young's modulus		34.0 GPa	SS 13 72 32/ NORDTEST NT 205 $E_0$ =CEB-FIP Definition $E_c$ =ISO 6784 Definition
Compression strength	after 1 day	C72/90	EN 196-1:1994
	after 7 days	23.3 MPa	20°C
	after 28 days	74.1 MPa	20°C
		92.3 MPa	20°C
Flexural strength	after 1 day	4.1 MPa	EN 196-1:1994
	after 7 days	10.4 MPa	20°C
	after 28 days	11.5 MPa	20°C
Pull out test - steel cylinder smooth bar	after 1 day	3.9 MPa	Pr EN 1881-1
	after 28 days	8.3 MPa	20°C
	after 1 day	-	5°C
	after 28 days	6.7 MPa	5°C
	after 1 day	4.1 MPa	35°C
	after 28 days	7.0 MPa	35°C
Pull out test - concrete cubes profiled bar	after 1 day	6.1 MPa	Pr EN 1881-1
	after 28 days	8.1 MPa	20°C
			20°C
Consistency by funnel	5 min	460 mm	No standard. Described in "Betonghandboken Arbetsutförande 12:5.7.4"
	10 min	460 mm	
	30 min	420 mm	
Short term expansion		0%	ASTM C940
Bleeding		0%	ASTM C940
Shrinkage	after 28 days	>5°C	
	after 56 days	0.1%	
		0.11%	
Expansion		0.5-2%	
Curing		4 h	
Usage time		30 min	
Outdoor use		yes	
Texture		fluid	
Water proof		yes	SS 137214
Durability		yes	SS 137244 for salty environments
Chloride diffusion coefficient			Pr EN 13396
Shrinkage	84 days	0.11%	Pr EN 480-3
Swelling	84 days	0.02%	Pr EN 480-3
Thermal expansion	84 days	10.6 $\mu\text{m}/(\text{m}^\circ\text{C})$	EN 1770

Table 4.4: Concrete mixture from the technical specification in Table 4.3.

Component	[kg/m <sup>3</sup> ]
Cement	253.1
Aggregate (0-4 mm)	511.5
Water	235.4
Water-cement ratio	0.3

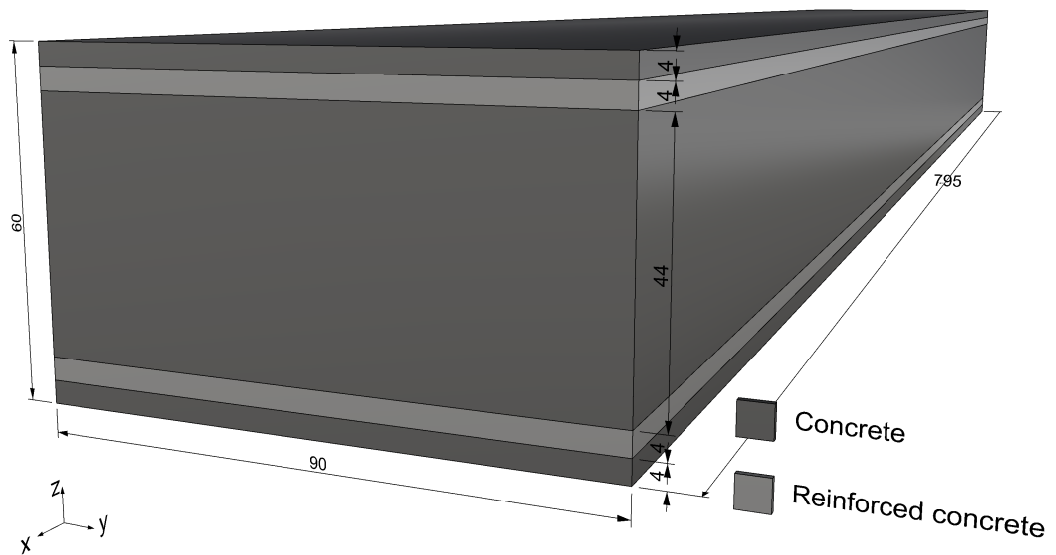


Figure 4.2: Illustration of the reinforced beam.

### 4.1.2 Composition of the Specimens

The beam specimen for this test were prepared by a formwork with the outer dimensions 800 mm x 100 mm x 150 mm, see Figure 4.8, giving a specimen size of 795 mm x 90 mm x 60 mm, see Figure 4.2. For easy removal of the formwork, oil was smeared on the inner sides of the formwork. The concrete mass was mixed 5 min by a concrete mixer until the mass became homogeneous. Apart from the concrete mixing, the application of reinforcement in the formwork involved only hand labour. The concrete mixture is shown in Table 4.4 and the technical specification could be read in Table 4.3.

The glass and carbon reinforcement textiles from Sto and the steel wire mesh from the laboratory were prepared by lay-up of four layers in the cement paste, at the bottom and top surfaces. Their material properties are shown in Table 4.5. The tensile strength of the TRC materials, see Table 4.1, have almost similar properties as the mentioned TRC materials in Hegger et al. (1998). Note that the reinforcement layers were densely stacked close to the upper and lower surfaces, see Figure 4.3. These beams, for this experimental test, are thicker than regular shell structures and they are reinforced with two layers, which is more similar to traditional concrete structures.

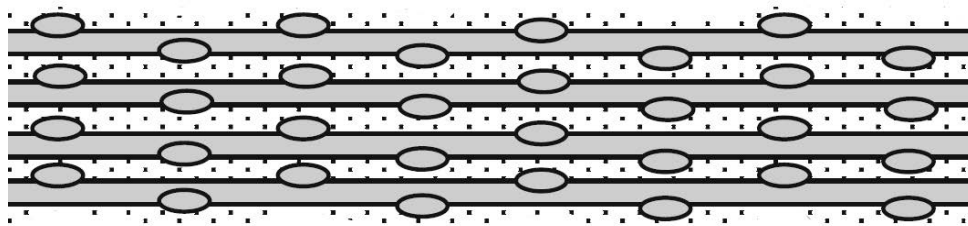


Figure 4.3: Section of thin concrete composite with several layers of mesh (grey). Source: Naaman (2012).

Table 4.5: Material properties of ferrocement, TRC and concrete.

	Area <sup>1)</sup> [mm <sup>2</sup> ]	Area <sup>2)</sup> [mm <sup>2</sup> ]	Mesh size [mm]	Layers [-]
Ferrocement	0.79	1	10	4
Glass TRC	1	1	7.5	4
Carbon TRC	3	3	38	4

1) Area of one wire or yarn.

2) Used in the numerical and analytical models.

In short, the concrete was cast in several batches in order to reach the right distance for the reinforcement within 4 mm, from the bottom and top edge. The formwork was marked by reference points on the inner sides with masking tape, see Figure 4.8. The reinforcement was applied 4 mm from the bottom and 4 mm from the top surface. The total height of the reinforced concrete beam was 60 mm, see Figure 4.2.

The casting process is dependent on which reinforcement material is used. The concrete mass was first cured 10 min at the bottom before the application of the TRC reinforcement and then 10 min at the top surface. Due to the higher density of the steel reinforcement, the steel wires were resting on 4 mm thick concrete distances in order to not sink to the bottom of the formwork during the vibration of the concrete. As shown in Figure 4.8, the top part was prevented from moving by anchoring the ferrocement with wires connected to the formwork. Finally, in order to remove air pores the concrete was vibrated approximately 1 min on a vibrating table.

### 4.1.3 Method of Testing

The beams were cured by first immersing them in a water tank for five days, and then by air drying them for 23 days under a sheet of plastic. The curing process thus lasted for a total of 28 days. The dimensions of the beam specimen after hardening were 795 mm x 90 mm x 60 mm (height error of  $\pm 10$  mm).

The specimens were tested in a loading frame (max capacity 100 kN and with an error of 10 N) under displacement control. In order to keep a good testing surface, the beams were washed. Moreover, the locations of the supports, loading cell and LVDT (linear variable differential transformer) were measured and marked on the beam, in order to measure the deflection equally throughout the experiment. The LVDT was measuring the movement of its piston during loading, see Figure 4.4. The LVDT was used to measure the beam deflection and had an error of 0.03 mm. Figure 4.9 shows the experimental set-up.

The deflection of the beam at the applied load (200 mm from the support) is given by

$$\delta = \frac{Fa^2(3L - 4a)}{6EI} \quad (4.3)$$

where

- $F$  load over one steel plate  $F = \frac{P}{2}$
- $a$  distance from support to load
- $L$  total beam length
- $E$  Young's modulus
- $I$  moment of inertia

The deflection measured in the mechanical test is in fact not the deflection of the beam. Hence, there are some error deviations, since the testing machine is deforming. In order to determine the actual stiffness of the beam, the deflection from the testing machine must be subtracted.

By viewing the machine set-up as a serial spring model (Figure 4.9) the correct deflection may be determined. The spring system has two springs connected to each other, one for the machine ( $k_1$ ) and a second for the beam ( $k_2$ ), see Figure 4.9. The total spring system is described as  $k_{tot}$ , see Equation 4.4,

$$\frac{1}{k_{tot}} = \frac{1}{k_1} + \frac{1}{k_2} \quad (4.4)$$

where,

$$k = \frac{P}{\delta}. \quad (4.5)$$

In this case, a steel beam (IPE160) was used to determine the stiffness of the machine. The  $k_{mean}$ , in the Figure 4.10, is the mean value of the two tests that was done,  $k_{test A}$  and  $k_{test B}$ . The subtracted values from the total displacement are calculated by the relationship (4.5) of the force  $P$  and the stiffness of the testing machine,  $k_1$ . See the stiffness values for the beam in Figure 4.10.

During loading, each beam was inspected visually for the first crack formation (state I, which is also called  $P_c$ ), so as to estimate the strength at the first crack. The specimens were tested to failure to obtain their ultimate strength ( $P_u$ ). The measuring equipment was connected to a computer that could plot the load-deflection behaviour.

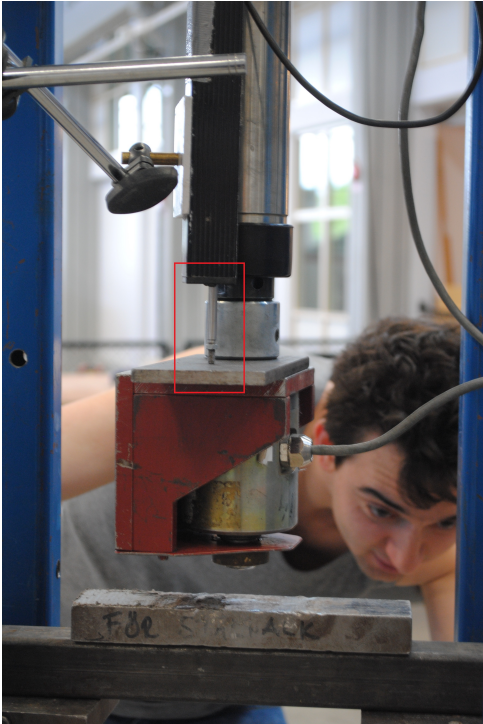


Figure 4.4: LVDT piston (red).



Figure 4.5: Machine set-up.



Figure 4.6: The reinforcement specimen: steel, glass and carbon fabrics. From the left-hand side steel, glass and carbon.

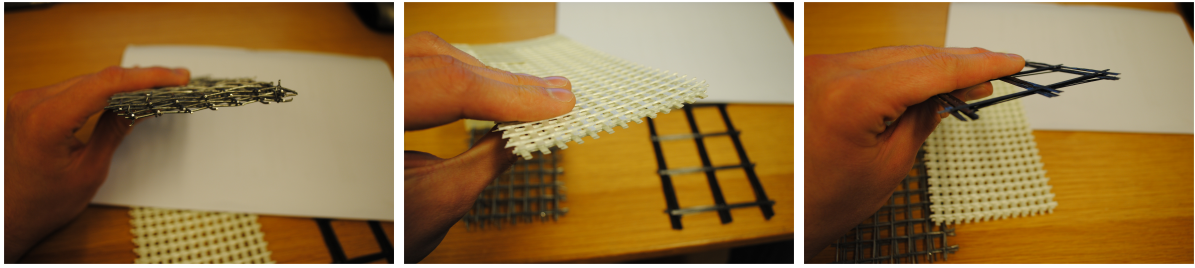


Figure 4.7: Section view of the reinforcement specimen. From the left-hand side steel, glass and carbon.



Figure 4.8: Anchored steel reinforcement in formwork.

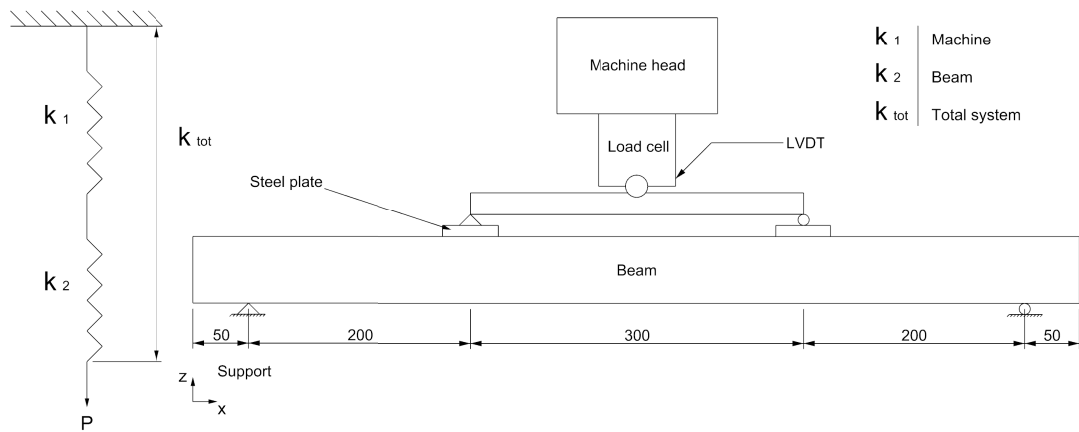


Figure 4.9: Schematic test set-up for four-point bending test. The axial point load  $P$  is the applied force from the load cell.

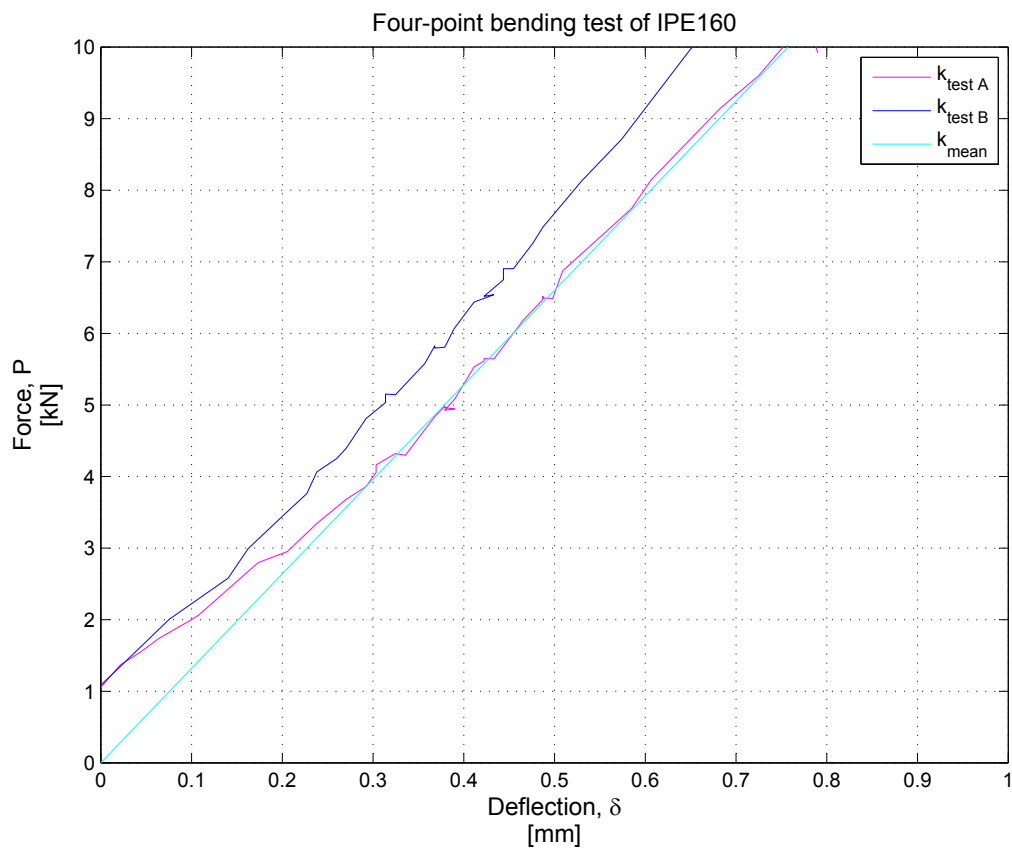


Figure 4.10: Stiffness model of the steel beam (IPE160) test set-up, where  $k_{mean} = 13.205$ , which is the mean value of  $k_{test A}$  and  $k_{test B}$ .

## 4.2 Results

The preparation of the reinforcement installation took the longest time. Especially for steel, with a preparation time of fifteen hours, as shown in Table 4.7. The concreting took approximately seven hours.

The penetration of the concrete gravels appeared to be good, which is shown in Figure 4.11-4.13. The final result of the beam stiffness is given in Table 4.6.

Furthermore, the behaviour during loading was investigated for the nine beam specimens with a four-point bending test. The beams were showing typical bending cracks between the steel plates, see Figure 4.14. The first crack ( $P_c$ ) for the nine beams occurred for a load of 5 kN. The ultimate crack failure ( $P_u$ ) was reached for the glass fibre reinforced beam at 10-14 kN. In addition, the crack load for the ferrocement and carbon reinforcement were approximately the same, about 7-10 kN. The graphs in Figure 4.15 of the steel reinforcement shows a clear ductility, due to its characteristic yielding behaviour.

Table 4.6: Results from the mechanical experiment. The amount of reinforcement are calculated for the whole beam.

	Amount <sup>1)</sup> [%]	$P_c$ [kN]	$P_u$ [kN]	$\delta$ [mm]	$k_{beam}$ <sup>2)</sup> [kN/mm]
Ferrocement	1.83	4.07	8.45	7.38	11.32
Glass TRC	3.34	4.30	12.46	10.72	5.57
Carbon TRC	2.14	4.57	9.74	11.23	7.57

1) Volume percentage of the reinforcement materials.

2) Stiffness is equal to  $\frac{P}{\delta}$ .

Table 4.7: Labour activity in constructing formwork.

Work	Hours
Steel RC <sup>1)</sup> installation	15
Glass TR <sup>2)</sup> installation	1
Carbon TR installation	1
Concreting	7
De-moulding	1
Mechanical testing	7
Total	32

1) RC – reinforcement concrete.

2) TR – textile reinforcement.



Figure 4.11: Section cut of a steel reinforced beam (beam C).



Figure 4.12: Section cut of a glass reinforced beam (beam E).



Figure 4.13: Section cut of a carbon reinforced beam (beam G).



Figure 4.14: Bending cracks of the nine beam specimen.

### 4.3 Discussion

Figure 4.14 illustrates clear bending cracks within the loading span of the beams, which are appropriate results from the mechanical test. In addition, their crack behaviour in the middle, is clearly explained in the Figure 4.15-4.17. Hence, the expected linear behaviour was found for all of the nine specimens. The linear part of the curves, in Figure 4.15-4.17, determines the material stiffness properties for the test specimens. Their stiffness are shown in Table 4.6.

The crack formation in the first state (so-called state I) for the nine specimen appeared at about 5 kN, which is a sufficient value due to the concrete tensile strength. The glass and carbon specimen (D-I) in Figure 4.14 do not yield, since pure crack formations are increasing up to the crack failure. The crack behaviour for the TRC fabrics was more sudden and unexpected than for ferrocement. Compared to the both TRC fabrics, ferrocement was yielding during the second state and failure was reached at about 8 kN load.

The third state ( $P_u$ ) for the carbon reinforced beam was that it occurred at 10 kN and for the glass reinforced beam between 10-14 kN. The failure differences for the glass reinforced beam depends probably on which position the beam crack appeared at. As already mentioned, the failure for ferrocement occurred at 8 kN. The concrete stones for the displacement of the steel mesh were placed in the middle of the formwork, which could have affected the results.

Carbon has the highest tensile strength of the three reinforcing materials. However, the crack failure for the glass was much higher than for carbon TRC. Ferrocement has more reinforcing material per sectional area, hence it has the highest stiffness comparing with the glass and carbon TRC. As a conclusion, the reason why there is such a difference in stiffness from the tests, is probably the amount of reinforcing material per sectional area for ferrocement and glass compare with the carbon TRC.

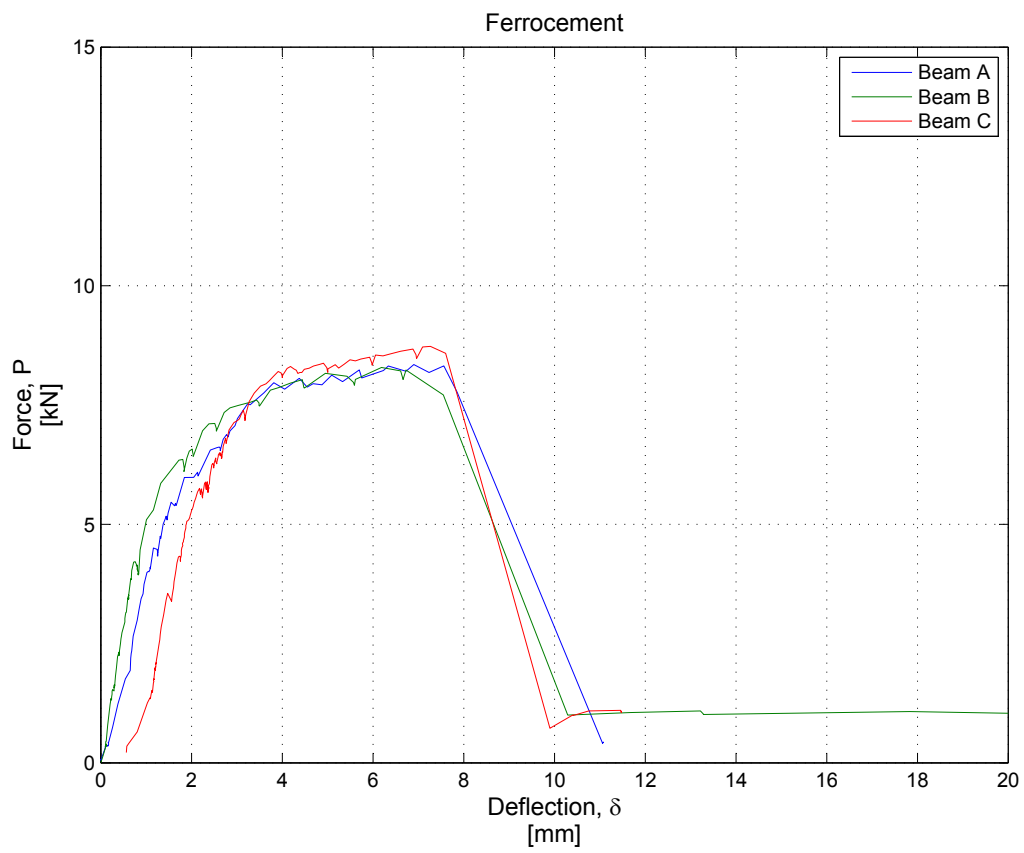


Figure 4.15: Force-deflection graph of the steel reinforced beam from the mechanical tests.

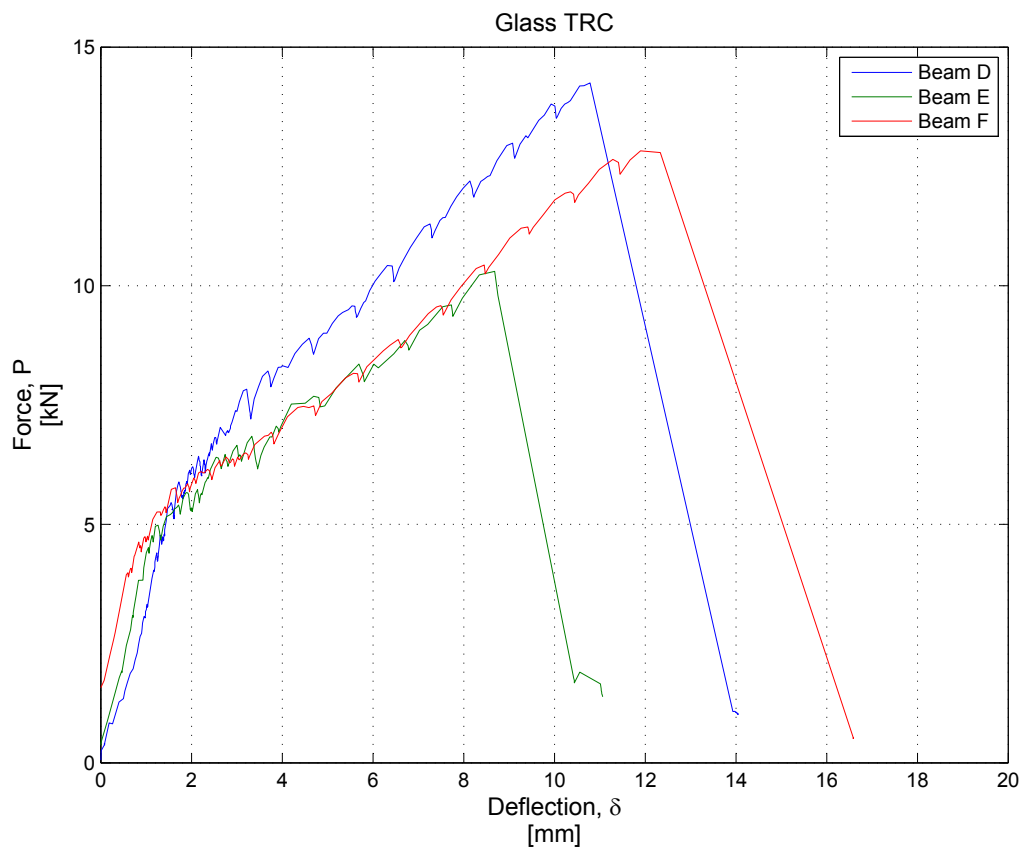


Figure 4.16: Force-deflection graph of the glass reinforced beam from the mechanical tests.

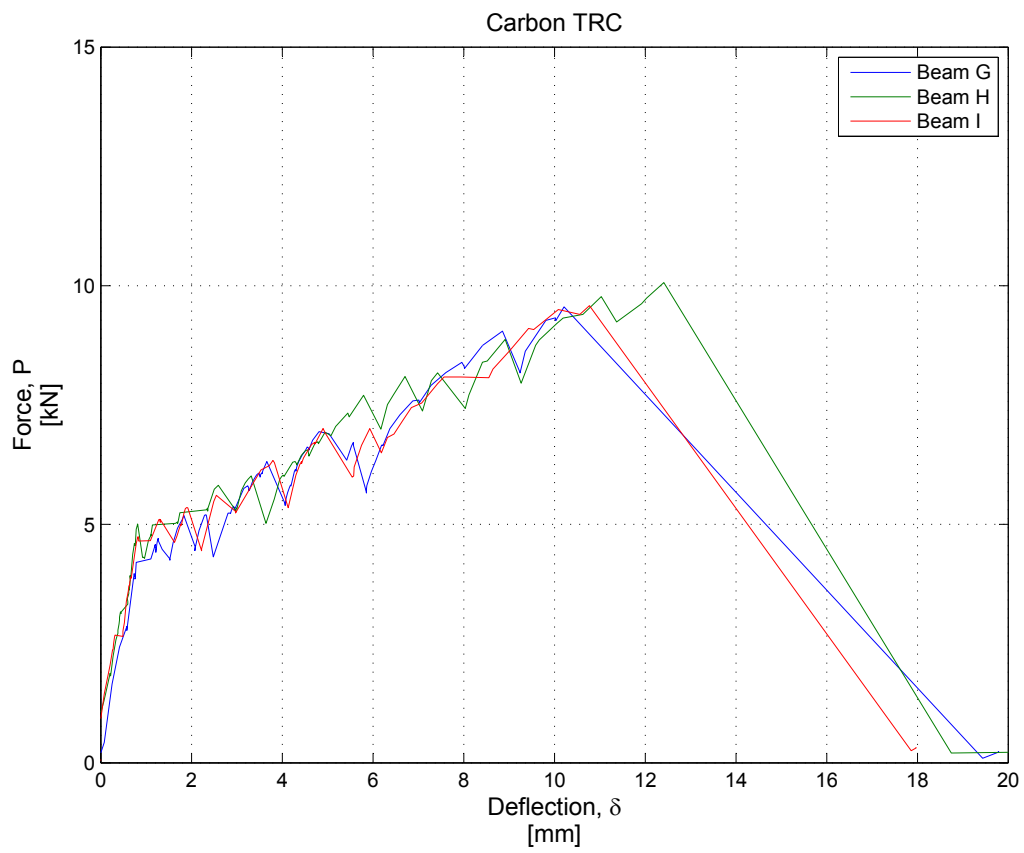


Figure 4.17: Force-deflection graph of the carbon reinforced beam from the mechanical tests.

# Chapter 5

## Finite Element Model

Physical phenomena can in most cases be described by differential equations. For more complex geometries solution to these equations may not be available. Solutions could, however, be achieved by using a numerical method, such as, the finite element method (FEM) (Ottosen Saabye and Petersson, 1992).

Three representative volume element (RVE) models are used in this chapter. The first one is ferrocement and the second and third one are glass and carbon TRC. FE models have for this reason been useful to solve the equivalent stiffness properties of these composite materials.

### 5.1 Finite Element Method

The differential equations that described the structural mechanical problems are assumed to hold over a certain region. Instead of searching for approximations for the whole region, the model is divided into smaller parts, called finite elements (FE). Approximations are made for the elements, which could be linear or quadratic elements. The elements are then assembled to describe the entire region. The assembled finite element can assume the variation over the entire region of the variables from a non-linear to a linear manner (Ottosen Saabye and Petersson, 1992). Such an assembled element is called finite element meshes.

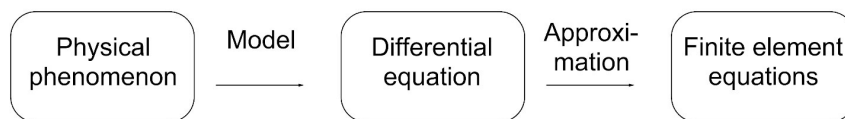


Figure 5.1: Analysis scheme from physical phenomenon to FEM.

Furthermore, the FE method can be utilised in many applications, e.g. to solve differential problems such as heat conduction, flexural behaviour and plates. The information of the material properties, boundary conditions and geometry, is given by a so-called  $\mathbf{K}$ -matrix, representing the stiffness of the whole system.

### 5.1.1 Linear Elastic Analysis

The relation between stresses and strains is called the constitutive relation (Ottosen Saabye and Petersson, 1992). In one dimension, linear elasticity is expressed by Hooke's law from 1676,

$$\sigma = E\varepsilon \quad (5.1)$$

where the Young's modulus  $E$ , is the material constant.

Hooke's law may be generalised to three dimensions by the constitutive matrix  $\mathbf{D}$ , which is called the Cauchy elasticity (Cauchy, 1789-1857), see Equation 5.2.

$$\sigma = \mathbf{D}\varepsilon \quad (5.2)$$

The  $\mathbf{D}$ -matrix has 36 elasticity coefficients, but since there is a symmetry the coefficients are reduced to 21 independent coefficients. The structure of the constitutive matrix  $\mathbf{D}$  is dependent on the material properties. It can either describe an anisotropic, isotropic, transverse isotropic or orthotropic material.

One important characteristic of an orthotropic material is that it has three principal orthogonal directions;  $x$ ,  $y$  and  $z$ , which also are called planes. Each symmetry plane consists of two coordinate systems. The  $\mathbf{D}$ -matrix is unchanged, if the two coordinate systems are mirror images of each other with respect to this plane. In an orthotropic plane the coordinates are parallel to these planes. Concrete is classified as an orthotropic material referring to its irregular microstructure. The  $\mathbf{D}$ -matrix for an orthotropic material is

$$\sigma = \begin{bmatrix} \sigma_{11} \\ \sigma_{22} \\ \sigma_{33} \\ \sigma_{12} \\ \sigma_{13} \\ \sigma_{23} \end{bmatrix}; \mathbf{D} = \begin{bmatrix} D_{1111} & D_{1122} & D_{1133} & 0 & 0 & 0 \\ D_{2211} & D_{2222} & D_{2233} & 0 & 0 & 0 \\ D_{3311} & D_{3322} & D_{3333} & 0 & 0 & 0 \\ 0 & 0 & 0 & D_{1212} & 0 & 0 \\ 0 & 0 & 0 & 0 & D_{1313} & 0 \\ 0 & 0 & 0 & 0 & 0 & D_{2323} \end{bmatrix}; \varepsilon = \begin{bmatrix} \varepsilon_{11} \\ \varepsilon_{22} \\ \varepsilon_{33} \\ \gamma_{12} \\ \gamma_{13} \\ \gamma_{23} \end{bmatrix}. \quad (5.3)$$

## 5.2 Abaqus

The FEM software Abaqus has been used to model and analyse the RVE models, since the RVE models give the material properties of the ferrocement and textile reinforcement materials. This was necessary in order to determine the stiffness properties for the entire composite beams from the mechanical tests.

As a consequence, different assumptions in the program may affect the final result. Abaqus FEA solves static and dynamic FE problems for two and three-dimensional objects. The software that were used in this thesis are called Abaqus CAE and Abaqus Standard. Abaqus CAE is used for modelling and visualising the model in a pre and post-processing stage. In contrast to Abaqus CAE, the Abaqus Standard is used to run the actual model analysis (Abaqus 6.14, 2015).

The script language, Python, has been used as a direct input to Abaqus Standard to obtain an efficient workflow. Python is a programming language, which supports multiple programming paradigms including object-oriented, imperative and functional programming. Abaqus is one of the software that is supported by Python.

## 5.3 Equivalent Models: RVE

As mentioned, an RVE model, is aimed at determining the equivalent stiffness properties of ferrocement and TRC. The numerical investigations simulate the influence of reinforcing material as a composite material in concrete. However, since the RVE is modelled with various geometries and different material properties for the reinforcement, the final equivalent material will have different orthotropic matrix structures. The matrix structure  $\mathbf{D}$  in Equation 5.3 is defined as an orthotropic material, which is proposed in this case.

### 5.3.1 Geometry

The geometry of the RVE models is very simple. Hence, it is a small part of the lower (or upper) section of the real beam structure that was tested (see the RVE models in Figure 5.2). In short, its geometry is similar to a cube with reinforcement bars in both  $x$  and  $y$ -directions.

The three RVE models have the same height, which is totally 8 mm. The RVE models has different lengths and widths, due to the various mesh sizes of the ferrocement and the textile fabrics. The first four millimetres was consisting of pure concrete and the rest of the four millimetres of composite material, which was concrete and reinforcement bars. The round shape of the cross-section of the reinforcement bars was modelled square shaped in order to create sufficient connections between the bars, see Figure 5.2.

### 5.3.2 Material and Mesh

The material properties, Young's modulus and Poisson's ratio for the RVE models, were determined by the manufacturers Sto and Weber, except steel. The stiffness modulus for steel was chosen to 200 GPa. Note that the stiffness of the concrete is the characteristic value from the manufacturer. The properties of the materials are given in Table 5.1.

The meshes for the RVE models, which were quadratic elements, are defined by iterating until the assumption gives an equally distributed quadratic mesh. The mesh was 0.0005 m for ferrocement. Further on, for the textiles, the element sizes were for glass 0.00019 m and for carbon 0.0015 m, respectively. In order to calculate the orthotropic  $\mathbf{D}$ -matrices, a Python-script was implemented in Abaqus.

Table 5.1: Material properties for the Abaqus models.

Material	$E$ [GPa]	$\nu$ [-]
Steel	200	0.30
Glass	75	0.22
Carbon	242	0.20
Concrete	34	0.20

where

- $E$  Young's Modulus
- $\nu$  Poisson's ratio

Table 5.2: Mesh size of the Abaqus models.

Material	Mesh size [m]
Ferrocement	0.0005
Glass TRC	0.00019
Carbon TRC	0.0015

### 5.3.3 D-matrix

The  $\mathbf{D}$ -matrices were calculated by setting the strain to one,  $\varepsilon_{11} = 1$  and  $\varepsilon_{22} = \varepsilon_{33} = \gamma_{12} = \gamma_{13} = \gamma_{23} = 0$ , see the matrices in (5.5). Where,

$$\boldsymbol{\sigma} = \mathbf{D}[1, :] \quad (5.4)$$

from

$$\boldsymbol{\sigma} = \begin{bmatrix} \sigma_{11} \\ \sigma_{22} \\ \sigma_{33} \\ \sigma_{12} \\ \sigma_{13} \\ \sigma_{23} \end{bmatrix}; \mathbf{D} = \begin{bmatrix} D_{1111} & D_{1122} & D_{1133} & 0 & 0 & 0 \\ D_{2211} & D_{2222} & D_{2233} & 0 & 0 & 0 \\ D_{3311} & D_{3322} & D_{3333} & 0 & 0 & 0 \\ 0 & 0 & 0 & D_{1212} & 0 & 0 \\ 0 & 0 & 0 & 0 & D_{1313} & 0 \\ 0 & 0 & 0 & 0 & 0 & D_{2323} \end{bmatrix}; \boldsymbol{\varepsilon} = \begin{bmatrix} 1 \\ 0 \\ 0 \\ 0 \\ 0 \\ 0 \end{bmatrix} \quad (5.5)$$

will give

$$\boldsymbol{\sigma} = \begin{bmatrix} \sigma_{11} \\ \sigma_{22} \\ \sigma_{33} \\ \sigma_{12} \\ \sigma_{13} \\ \sigma_{23} \end{bmatrix} = \begin{bmatrix} D_{1111} \\ D_{2211} \\ D_{3311} \\ 0 \\ 0 \\ 0 \end{bmatrix}. \quad (5.6)$$

Furthermore, the second column of the matrix elements in matrix  $\mathbf{D}$  are calculated by applying strains as  $\varepsilon_{22} = 1$  and  $\varepsilon_{11} = \varepsilon_{33} = \gamma_{12} = \gamma_{13} = \gamma_{23} = 0$ . Then the rest of the columns in the  $\mathbf{D}$ -matrix are determined in the same manner.

The Python script creates the boundary conditions for  $\boldsymbol{\varepsilon}$ , runs the analysis and finally integrates the stresses  $\boldsymbol{\sigma}$ . The  $\mathbf{D}$ -matrices given below, are input data for the orthotropic section of the numerical beam model, see the  $\mathbf{D}$ -matrices (5.7), (5.8) and (5.9).

#### Ferrocement

$$\mathbf{D} = \begin{bmatrix} 41.942 & 10.147 & 10.120 & 0 & 0 & 0 \\ 10.147 & 41.894 & 10.102 & 0 & 0 & 0 \\ 10.120 & 10.102 & 39.786 & 0 & 0 & 0 \\ 0 & 0 & 0 & 14.925 & 0 & 0 \\ 0 & 0 & 0 & 0 & 14.938 & 0 \\ 0 & 0 & 0 & 0 & 0 & 14.909 \end{bmatrix} 10^9 \quad (5.7)$$

Glass TRC

$$\mathbf{D} = \begin{bmatrix} 40.170 & 9.975 & 9.982 & 0 & 0 & 0 \\ 9.975 & 40.137 & 9.968 & 0 & 0 & 0 \\ 9.982 & 9.968 & 39.693 & 0 & 0 & 0 \\ 0 & 0 & 0 & 14.878 & 0 & 0 \\ 0 & 0 & 0 & 0 & 14.870 & 0 \\ 0 & 0 & 0 & 0 & 0 & 14.878 \end{bmatrix} 10^9 \quad (5.8)$$

Carbon TRC

$$\mathbf{D} = \begin{bmatrix} 43.470 & 10.358 & 10.022 & 0 & 0 & 0 \\ 10.358 & 43.285 & 9.992 & 0 & 0 & 0 \\ 10.022 & 9.992 & 39.601 & 0 & 0 & 0 \\ 0 & 0 & 0 & 14.809 & 0 & 0 \\ 0 & 0 & 0 & 0 & 14.864 & 0 \\ 0 & 0 & 0 & 0 & 0 & 15.271 \end{bmatrix} 10^9 \quad (5.9)$$

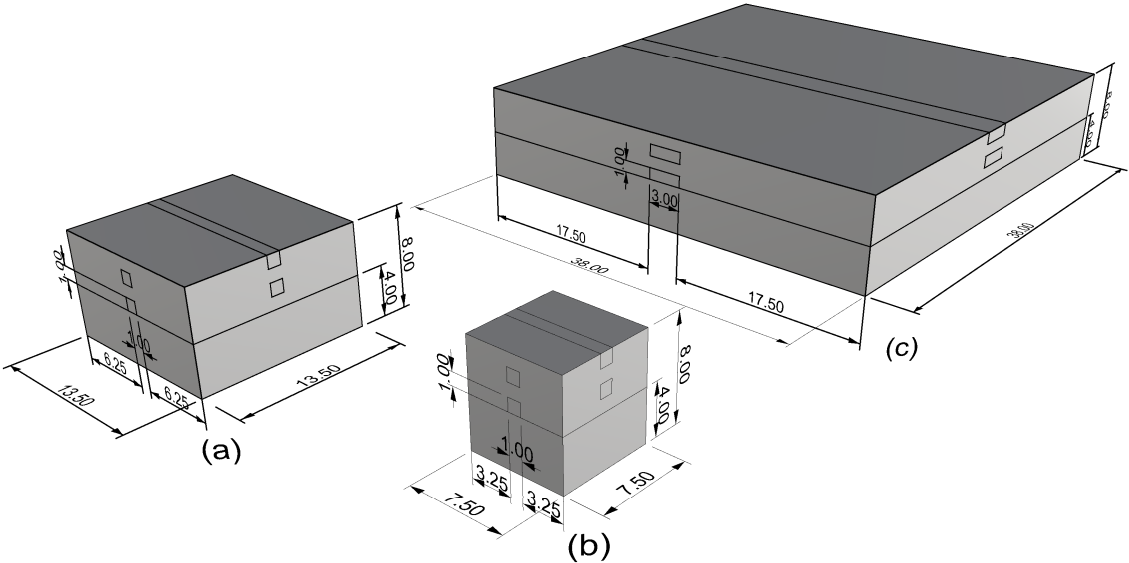


Figure 5.2: RVE models of ferrocement (a), glass (b) and carbon (c) TRC.

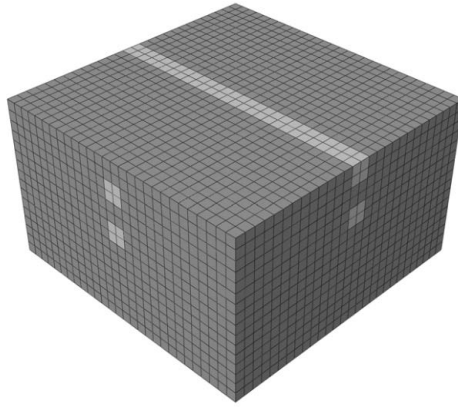


Figure 5.3: Mesh of the RVE ferrocement model (a).

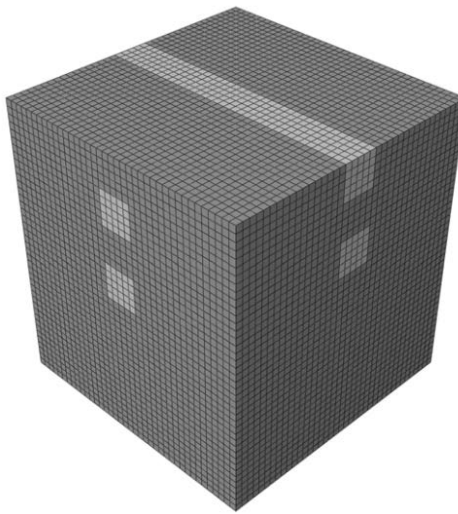


Figure 5.4: Mesh of the RVE glass TRC model (b).

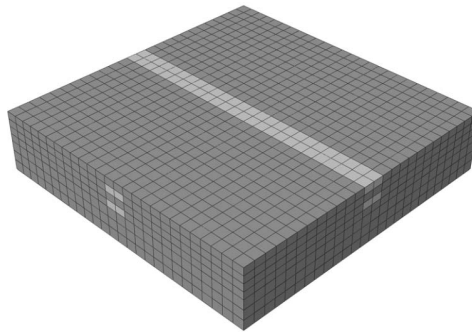


Figure 5.5: Mesh of the RVE carbon TRC model (c).



# Chapter 6

## Numerical Study of Mechanical Testing

The equivalent stiffness properties determined by the RVE model presented in Chapter 5 was used in models of the tested beams. In the following chapter, a numerical study of the beams from the mechanical tests will be presented, including a method of analysis and a part for discussion.

### 6.1 Finite Element Model

The FE study was performed by modelling the four-point bending test. The beam had the dimensions 0.700 m x 0.100 m and a height of 0.060 m. It was simply supported, with the effective span of 0.700 m. Two line loads were applied on top of the beam. The applied line loads were acting in the negative  $z$ -direction along two steel plates with the dimensions 0.050 m x 0.100 m x 0.010 m. The plates were assembled 0.200 m from the support.

Furthermore, the numerical beam model was divided into two sections: an orthotropic and isotropic section. The orthotropic section is the non-homogeneous part, which constitutes the bottom and top part of the beam. Its stiffness properties are determined from the numerical calculations of the RVE model. The isotropic part is the second part, an interlayer. The interlayer is modelled as pure concrete with the material properties shown in Table 5.1.

#### 6.1.1 Loads and Boundary Conditions

Since the beam was simply supported, the boundary conditions in the  $x$ -direction and the  $z$ -direction were set to zero ( $u_x = u_z = 0$ ). In order to prevent movement of the beam body, a point on the corner on the same side was set to  $u_y = 0$ . The opposite edge of the beam was constrained in the  $z$ -direction ( $u_z = 0$ ), see Figure 6.1.

Further on, the stiffness of the numerical beam was tested with and without steel plates in order to see if the steel plates gave great stiffness deviations. The boundary condition for the applied load was, as already mentioned, set in the negative  $z$ -direction. The interaction between the steel plate and the beam was set to be merged, without allowing any movements in the connection.

#### 6.1.2 Step and Mesh

Only one step was created, the general static. In a general static step, the stresses are determined with no account taken of the creep of the interlayer between the concrete and composite section. The quadratic mesh size was set to 0.005 m x 0.005 m, see Figure 6.2.

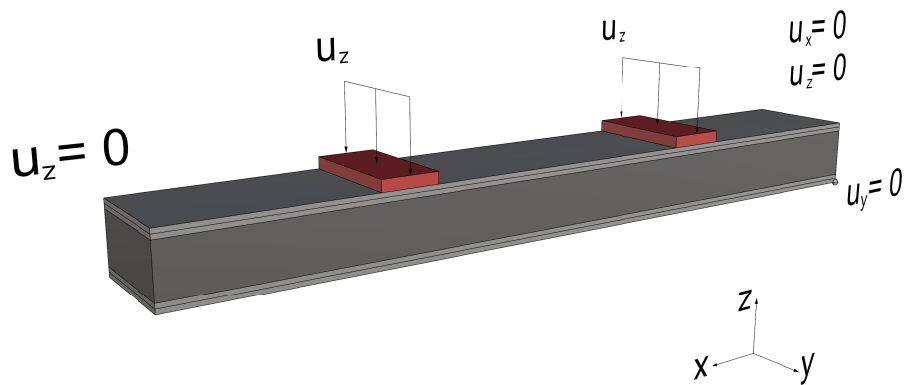


Figure 6.1: The load and boundary conditions for the beam model. Steel plate (red).

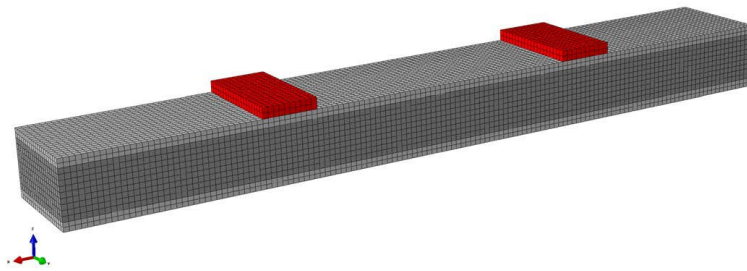


Figure 6.2: The mesh of the beam model.

## 6.2 Results

The forces and displacements were imported to MATLAB. The results from the numerical model were collected from where the total force  $P$  was applied. The stiffness is given by the quotient of the force,  $P$  and the displacement,  $\delta$ , see Table 6.1. Furthermore, there are differences in stiffness of a pure concrete beam with or without a steel plate. Since, there is a deviation of 4.4% between alternative 2) and 3) in Table 6.1.

Table 6.1: Stiffness from the mechanical and numerical model.

	Numerical model $k_{numerical}^{1)}$
Pure concrete <sup>2)</sup>	14.12
Pure concrete <sup>3)</sup>	14.74
Ferrocement	15.57
Glass TRC	15.15
Carbon TRC	15.94

1) Stiffness illustrated in Figure 8.1.

2) With steel plates.

3) Without steel plates.

### 6.3 Discussion and Comparison with Mechanical Testing

Just as the Table 6.2 shows, there is a significant difference between the stiffness values from the mechanical experiment and the numerical study. For this reason, the numerical model can not verify the stiffness from the experimental tests. The results from the numerical model, which is shown in Table 6.2, show that the stiffness of the numerical model is two to three times higher than the stiffness of the mechanical results. The greatest stiffness deviations are for the TRC materials, which is 272% for glass and 211% for carbon. The stiffness deviation for ferrocement is much less, only 38%. The stiffness does not vary if the beam is assembled with or without a steel plate, which can be seen in Table 6.1.

One of the explanations due to the stiffness deviation between the mechanical model and the numerical model, could be the bonding strength (adhesion) between the reinforcement and the concrete. Since, small cracks close to the reinforcement could appear due to the low bonding strength. This could induce stress concentrations in those areas, which can influence the stiffness from the mechanical experiment. Another explanation could be constructional tolerances. This include how the beams were prepared, constructed and tested.

The mechanical result could also be affected by the addition of water, mixing and vibrating the concrete mass. Other explanations, could be the undefined technical specification for the steel wire. This forced the experiment to use an approximate value from the literature for the steel properties. Some deviations could also be explained by the thickness variations of the beam in the  $z$ -direction. The thickness varies between 6.5-8.1 mm. This could probably be one of the most important reasons to the stiffness deviations.

Table 6.2: Stiffness from the mechanical test and numerical model.

	Mechanical test $k_{beam}$	Numerical model $k_{numerical}$	Deviation <sup>1)</sup> [%]
Pure concrete	-	14.59	-
Ferrocement	11.32	15.57	38
Glass TRC	5.57	15.15	272
Carbon TRC	7.57	15.94	211

1) Deviation between the  $k_{beam}$  and  $k_{numerical}$ .



# Chapter 7

## Analytical Study of Numerical Model

The purpose of this chapter is to study two analytical models: an RVE model and a model for the beam stiffness. Serial and parallel models will be used for analysis of the RVE model and stiffness calculations will be applied for analysing the beam stiffness. Discussions and comparison will be mentioned at the end of this chapter.

### 7.1 Stiffness of the Beam

In order to verify the stiffness from the mechanical test, an analytical analysis of the beams is sufficient in this kind of study. The stiffness is determined by

$$k_{analytical} = \frac{P}{\delta}. \quad (7.1)$$

The deflection  $\delta$  is calculated by the deflection formula (7.2) for a four-point bending test.

$$\delta = \frac{Fa^2(3L - 4a)}{6EI} \quad (7.2)$$

Furthermore, the stiffness  $EI$  is the stiffness for the ferrocement beams, glass and carbon TRC beams, which were used in the mechanical test. Regarding the orientation of the fibres, assumptions has been made that the fibres are placed 6 mm from the edge in the middle of the beam, see Figure 7.1b. In this case they are determined by

$$EI = E_c I_c + 2E_r I_r \quad (7.3)$$

where

- $c$  concrete index
- $r$  reinforcement index

see the calculations in Table A.1 and A.2 in Appendix.

Note, that the stiffness  $EI$  only describes the actual geometry and the amount of material, concrete and reinforcement. In addition, the mechanical model is simplified by an analytical model, as shown in Figure 7.1b. The stiffness  $k_{analytical}$  could then be determined for each of the three reinforced beams by using Equation 7.1. The results of the three different reinforced beams are shown in Table 7.1.

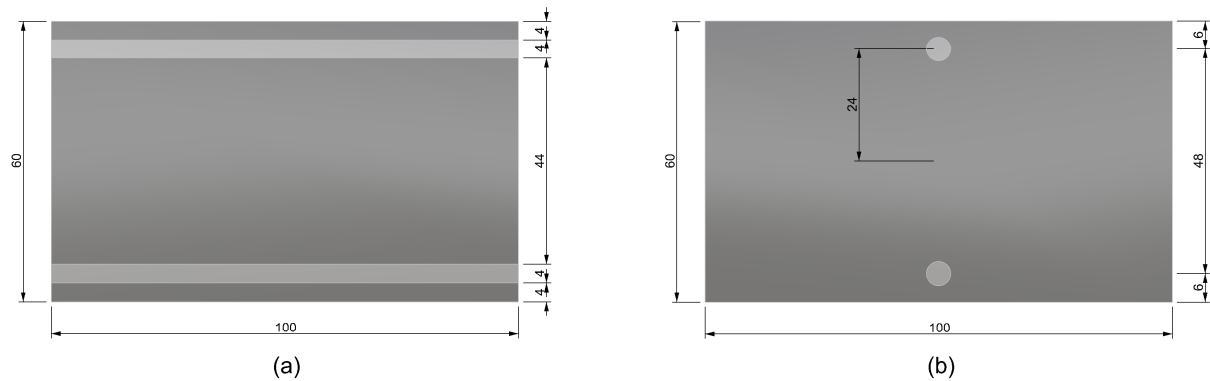


Figure 7.1: Assumption (b) of the reinforced beam (a) from the mechanical testing.

## 7.2 Mechanical Spring Models

When the load is applied in a composite material, the loads are transferred to the concrete and the textile materials. This system can be comparable with a spring system, either a serial or parallel model, which have different properties depending on in which direction the displacement,  $u$ , is applied.

This spring system, represents the linear elastic behaviour and gives the stiffness of the composite material. In other words, the stiffness  $S$ , of a composite material, is the relation between the actual stiffness of the concrete and the composite material. Hence, the spring system is represented by a linear elastic behaviour where the stiffness is given by the stated Hooke's law in Figure 7.2.

The comparison is conducted between the stiffness of the analytical serial and parallel model with the  $\mathbf{D}$ -matrices for the reinforcements in the RVE model. The diagonal matrix values  $D_{1111}$ ,  $D_{2222}$  and  $D_{3333}$  are the characteristic stiffness values to compare with the stiffness  $S$ . The  $S$ -stiffness values should be the interval values for the diagonal matrix values  $D_{1111}$ ,  $D_{2222}$  and  $D_{3333}$ . The serial and parallel models will be explained in the following Sections 7.2.1 and 7.2.2.

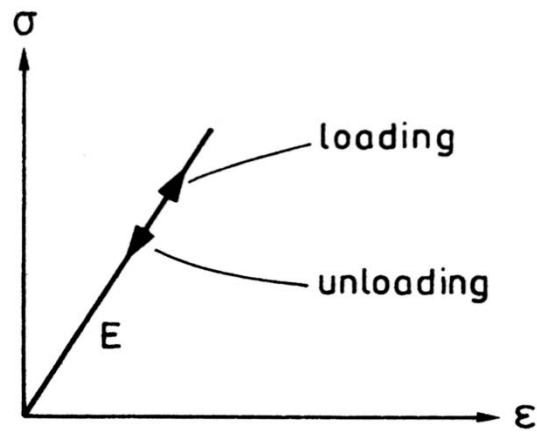


Figure 7.2: Linear elasticity (Ottosen Saabye and Petersson, 1992).

### 7.2.1 Serial Connected Model

The RVE model could be described as a serial and parallel model. Let us first start with the serial model and then go over to the parallel model. The serial model is a model where the displacement is applied perpendicular to the reinforcement direction. The spring system is collaborating in a serial manner (7.5), where only the length of the material is the significant variable.

$$k_{tot} = \frac{1}{k_1} + \frac{1}{k_2} \quad (7.4)$$

$$S_{ser} = \frac{L}{\frac{L_c}{S_c} + \frac{L_r}{S_r}} \quad (7.5)$$

where

- $c$  concrete index
- $r$  reinforcement index

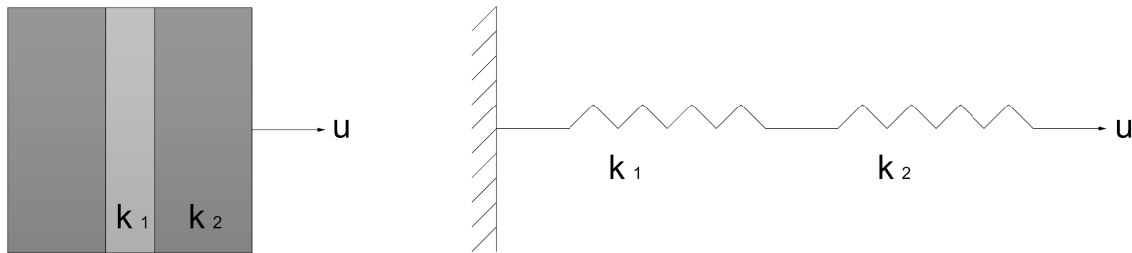


Figure 7.3: The serial spring model.

### 7.2.2 Parallel Connected Model

In contrast to the serial model, the parallel spring model (7.7) is a model where the displacement is applied along the direction of the reinforcement. This creates a parallel connected system, where the dependent factor is the area of the material.

$$k_{tot} = k_1 + k_2 \quad (7.6)$$

$$S_{par} = \frac{S_c A_c}{A} + \frac{S_r A_r}{A} \quad (7.7)$$

where

- $c$  concrete index
- $r$  reinforcement index

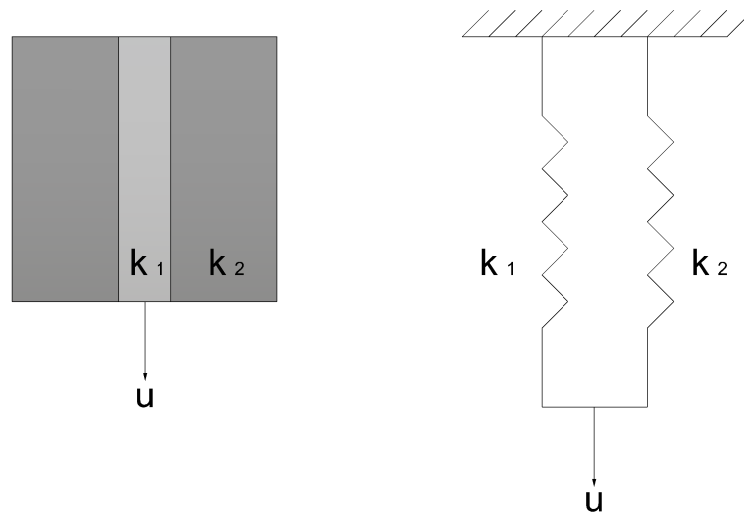


Figure 7.4: The parallel spring model.

### 7.3 Results

The results from the analytical model in Table 7.1 show that the carbon reinforced beam has the highest stiffness compare to the other stiffness values from glass TRC and ferrocement. The results for the serial and parallel model are shown in Table 7.3, where the results from the serial and parallel models are in good agreement with the actual **D**-stiffness in Chapter 5 (5.7), (5.8) and (5.9).

Table 7.1: Analytical stiffness calculations.

	$EI$ [kNm <sup>2</sup> ]
Ferrocement	66.267
Glass TRC	65.693
Carbon TRC	91.309

Table 7.2: Stiffness of the pure concrete beam and the three reinforcements.

	Analytical model $k_{analytical}^{1)}$
Pure concrete	14.12
Ferrocement	15.29
Glass TRC	15.16
Carbon TRC	21.07

1) Stiffness illustrated in Figure 8.1.

Table 7.3: Serial and parallel model results.

		Ferrocement [GPa]	Glass TRC [GPa]	Carbon TRC [GPa]
Serial model	$S_{ser}$	38.4	39.0	38.9
	$D_{1111}$	42.0	40.2	43.5
	$D_{2222}$	41.9	40.1	43.3
	$D_{3333}$	39.8	39.7	39.6
Parallel model	$S_{par}$	46.3	39.5	50.4

## 7.4 Discussion and Comparison with Numerical Model

The results from the analytical model show that the RVE stiffness values ( $D_{1111}$ ,  $D_{2222}$  and  $D_{3333}$ ) are the intermediate stiffness values between the serial and parallel model ( $S_{ser}$  and  $S_{par}$ ). Moreover, the deviation between the analytical and numerical model is 32% for carbon, which is much higher than the stiffness deviations for glass TRC and ferrocement. The deviation between the numerical and analytical model for ferrocement and glass TRC is 1.8% and 1.0% respectively, see Table 7.4.

The main reason of difference in stiffness for the carbon TRC compare to the ferrocement and glass TRC is the high Young's modulus of carbon (242 GPa). Carbon generally has a much higher stiffness than glass, which gives much higher analytical stiffness results for carbon. The stiffness deviations seem to be lower for ferrocement and glass TRC, as shown in Table 7.4. The stiffness values  $S_{ser}$  and  $S_{par}$  shall be close to Young's modulus of concrete (34 GPa), since the RVE models consist of 97-99% of concrete. Table 7.3 shows the stiffness values for the RVE model ( $D_{1111}$ ,  $D_{2222}$  and  $D_{3333}$ ) which are comparable to the analytical stiffness,  $S_{ser}$  and  $S_{par}$ .

Table 7.4: Stiffness from the numerical and analytical model.

	Numerical model $k_{numerical}$	Analytical model $k_{analytical}$	Deviation <sup>1)</sup> [%]
Pure concrete	14.59	14.12	3.2
Ferrocement	15.57	15.29	1.8
Glass TRC	15.15	15.16	1.0
Carbon TRC	15.94	21.07	32

1) Deviation between the  $k_{numerical}$  and  $k_{analytical}$ .

## Chapter 8

# Comparison of Ferrocement and TRC

### 8.1 Results

Table 8.1 shows the summary of the stiffness from the mechanical experiment, the numerical model and the analytical model. Table 8.1 is also illustrated in Figure 8.1. The deviations are shown in Table 6.2 and 7.4.

Table 8.1: Stiffness from the mechanical test, numerical and analytical model.

	Mechanical test $k_{beam}$	Numerical model $k_{numerical}$	Analytical model $k_{analytical}$
Pure concrete	-	14.59	14.12
Ferrocement	11.32	15.57	15.29
Glass TRC	5.57	15.15	15.16
Carbon TRC	7.57	15.94	21.07

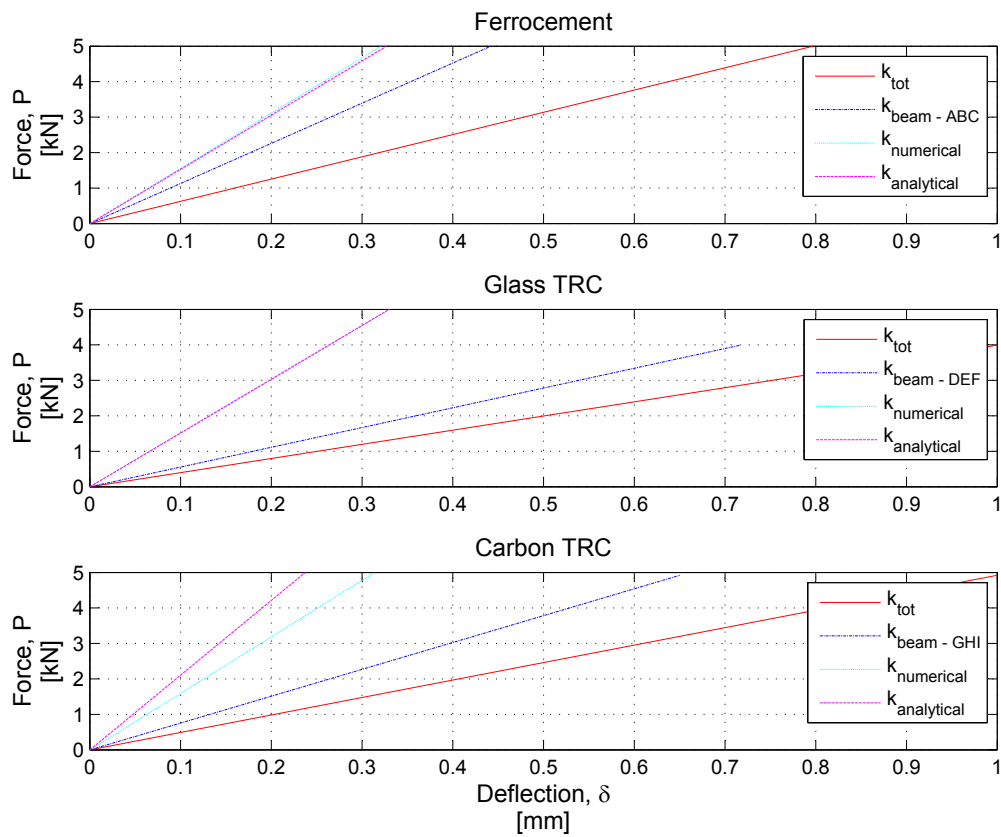


Figure 8.1: Comparison between the beam models from the mechanical experiment (ABC, DEF, GHI), numerical model and analytical model.  $k_{tot}$  is the stiffness of the total system, where the deflection deviation from the testing machine is included.

## 8.2 Discussion

In Chapter 6 and 7, many aspects are mentioned regarding the stiffness deviations between the mechanical, numerical and analytical studies, see Table 8.1. The results from the mechanical tests and the numerical studies showed great deviations in stiffness. One explanation is the mechanical behaviour between the concrete and textiles. The mechanical behaviour is difficult to model since the textile materials are connected in a complex manner to the concrete. Their complexity makes it difficult to give the interlayer appropriate boundary conditions.

The numerical studies could be improved by better knowledge of modelling the concrete cracks (inside the concrete structure) close to the reinforcement. In addition, the beams had different thickness, which affected the final beam stiffness in the mechanical tests. The modelling could also be improved by better knowledge of boundary conditions and by better assumptions of material properties.

If referring to the analytical and numerical results from Table 8.1, the carbon TRC may be the stiffest material. Though, the mechanical tests were not statistically significant, since there were too few beams tested. By conducting mechanical experiments in a correct manner, properties of the final material would be more valuable.



## Chapter 9

# Conclusion

Construction with woven fabrics of steel, glass and carbon is time-consuming. Especially steel fabric, due to its non-flexible behaviour. Steel is a stiff material, particularly when two or more steel grids are arranged together. Its stiffness makes it even more difficult to construct, compared to the flexible textile fabrics. Moreover, anchoring the reinforcement to the framework is another problem. There is a difficulty in anchoring the reinforcement at the right distance from the top or bottom edge. Another aspect is also the risk of movements of the reinforcement during the concrete vibration.

The conclusion from the comparison of ferrocement and TRC in the mechanical experiment is that the thickness of the concrete beams has a great influence on the beam stiffness. In addition, microcracks appear between the reinforcement and concrete, which also influence on the final stiffness of the beams.

The RVE modelling should be compared to non-linear models in order to simulate the TRC in a sufficient way. Better simulation can be accomplished by calibration and comparison with physical tests. For instance the isotropic and heterogeneous material, ferrocement, is typically densely stacked and therefore non-linear modelling would be useful.

According to the mechanical tests, the ferrocement has the highest stiffness value compared to the carbon and glass fibre beams, probably due to the better bonding between the steel reinforcement and the concrete. Results in Table 8.1 show that the carbon TRC is the stiffest material according to the analytical and numerical studies. Finally, the concrete has probably a lower Young's modulus compared to the stated technical specification for the concrete product. Consequently, a lower stiffness of the cast composite beam could be predicted.



## Chapter 10

# Suggestions for Further Research

The mechanical and numerical analyses are the first steps towards further research in ferrocement and TRC for shell structures. It is clear that a lot of work is required for the further development of this working method.

Regarding the influence of deflection of the loading frame, focus on the measuring technique and material application would be of interest. A better method of applying and anchoring the reinforcement would be necessary for this kind of experimental test. The influence of movement of the measuring equipment, such as the loading cell, may induce measurement errors, which possibly can affect the results.

Some effort should be made in finding a better interaction between the steel plate and the concrete beam for the numerical model. It is also of importance to identify the material properties of the reinforcement and concrete, for the numerical and mechanical model. Studies of the behaviour between the concrete and the textile reinforcement should also be executed from a more mechanical aspect. Furthermore, an obvious continuation of the work would be to assess the ultimate limit state (ULS), since only the service limit state (SLS) has been analysed in this thesis work. Finally, an extra mechanical test of a pure concrete beam should be performed to determine the actual stiffness modulus for the concrete material. With further development of the mechanical experiment, improvements of the test will be achieved.



# Bibliography

- Adriaenssens, S., Block, P., Veenendaal, D., Williams, C., 2014. *Shell Structures for Architecture: Form Finding and Optimization*. Taylor & Francis – Routledge, London.
- Arockiasamy, M., Castro, J. O., Gale, D. M., Guerra, A. J., 2009. Report on Ferrocement. *International Journal*, American Concrete Institute, 1-28.
- Blaauwendraad, J. and Hoefakker, J. H., 2014. *Structural Shell Analysis: Understanding and Application*. Springer Science+Business Media, Dordrecht.
- Engström, B., 2006. *Betongbyggnad*. Göteborg.
- Gries, T., Roye, A., Offermann, P., Engler, T., Peled, A., 1998. Textiles. 11-27.
- Grosse, C., 2007. *Advances in Construction Materials*. Springer, Stuttgart.
- Hartig, J. and Jesse, F., 2010. Evaluation of Experimental Setups for Determining the Tensile Strength of Textile Reinforced Concrete. *International RILEM Conference on Material Science*, 117-127.
- Hartig, J., Jesse, F., Schick Tanz, K., Häußler-Combe, U., 2012. Influence of experimental setups on the apparent uniaxial tensile load-bearing capacity of Textile Reinforced Concrete specimens. *Materials and Structures*, 433-446.
- Hegger, J. and Will, N., 1998. State of the Art Report – Textile Reinforced Concrete. 133-185.
- Hegger, J., Will, N., Bruckermann, O., Voss, S., 2006. Load-bearing behaviour and simulation of textile reinforced concrete. *Materials and Structures*, 765-776.
- Hertzell, T., Sjöström, J., Hellers, B., 2003. *Helgjutet: En bok om betonghus gjutna på byggsplatsen*. AB Svensk Byggtjänst, Stockholm.
- Marti, P., 2012. *Baustatik: Grundlagen, Stabtragwerke, Flächentragwerke*. Ernst & Sohn, Zürich.
- Mobasher, B., 2011. *Mechanics of Fiber and Textile Reinforced Cement*. Taylor & Francis Group, Boca Raton.
- Naaman, A., 2000. *Ferrocement and laminated cementitious composites*. Techno Press 3000.
- Naaman, A., 2012. Evolution in Ferrocement and Thin Reinforced Cementitious Composites. *Springer, Arabian Journal for Science and Engineering*, 37:421-441.
- Neville, A. and Brooks, J., 2010. *Concrete Technology*. Pearson Prentice Hall, Harlow.
- Otto, F., Rasch, B., Pfafferodt, G., Gräfin Schönborn, A., Schanz, S., 1996. *Finding Form: Towards an Architecture of the Minimal*. Deutscher Werkbund Bayern, München.
- Ottosen Saabye, N. and Petersson, H., 1992. *Introduction to the Finite Element Method*. Pearson Prentice Hall, Harlow.
- Petre, D. and Zapalowicz, I., 2012. Analysis of reinforced concrete slabs strengthened with textile reinforcement. *Division of Structural Engineering – Chalmers University of Technology, Göteborg*.
- Simulia, 2015. *Abaqus 6.14*. Simulia.
- Vogel, T., 2012. *Flächentragwerke*. Institut für Baustatik und Konstruktion – ETH, Zürich.



# Appendix A

## Appendix

Table A.1: Analytical calculations.

	$A_r$ [m <sup>2</sup> ]	$E_c$ [GPa]	$E_r$ [GPa]	$I_c$ [m <sup>4</sup> ]	$I_r$ [m <sup>4</sup> ]	$EI$ [Nm <sup>2</sup> ]
Ferrocement	$21.9 \cdot 10^{-6}$	34	200	$1.80 \cdot 10^{-6}$	$1.27 \cdot 10^{-8}$	66267
Glass TRC	$52.0 \cdot 10^{-6}$	34	75	$1.80 \cdot 10^{-6}$	$3.00 \cdot 10^{-8}$	65693
Carbon TRC	$108.0 \cdot 10^{-6}$	34	242	$1.80 \cdot 10^{-6}$	$6.22 \cdot 10^{-8}$	91309

Table A.2: Serial and parallel model results.

	$E_c$ [GPa]	$E_r$ [GPa]	$A_c$ [m <sup>2</sup> ]	$A_r$ [m <sup>2</sup> ]	$A$ [m <sup>2</sup> ]	$L_c$ [m]	$L_r$ [m]	$L$ [m]	$S_{ser}$ [GPa]	$S_{par}$ [GPa]
Ferrocement	34	200	$13 \cdot 10^{-6}$	$1 \cdot 10^{-6}$	$14 \cdot 10^{-6}$	$6.25 \cdot 10^{-3}$	$1 \cdot 10^{-3}$	$7.2 \cdot 10^{-3}$	46.3	38.4
Glass TRC	34	75	$6.5 \cdot 10^{-6}$	$1 \cdot 10^{-6}$	$7.5 \cdot 10^{-6}$	$3.25 \cdot 10^{-3}$	$1 \cdot 10^{-3}$	$4.25 \cdot 10^{-3}$	39.5	39.0
Carbon TRC	34	242	$35 \cdot 10^{-6}$	$3 \cdot 10^{-6}$	$38 \cdot 10^{-6}$	$17.5 \cdot 10^{-3}$	$3 \cdot 10^{-3}$	$20.5 \cdot 10^{-3}$	50.4	38.9

Table A.3: Beam height from the experimental test. Measurements were taken from the middle of the beam.

	Beam	Height [mm]	Deviation <sup>1)</sup> [%]
Ferrocement	A	7.0	29
	B	7.1	30
	C	7.3	27
Glass TRC	D	8.1	19
	E	6.8	32
	F	6.5	35
Carbon TRC	G	7.0	30
	H	6.9	31
	I	7.3	27

1) Deviation between the actual height and the numerical beam height (100 mm).

